Available online at www.sciencedirect.com
SCIENCE DIRECT®
Remote Sensing of Environment 99 (2005) 271 – 287
Remote Sensing of Environment
www.elsevier.com/locate/rse

Assessing vineyard condition with hyperspectral indices: Leaf and canopy reflectance simulation in a row-structured discontinuous canopy

P.J. Zarco-Tejada [a,*], A. Berjón [b], R. López-Lozano [c], J. R. Miller [d], P. Martín [e], V. Cachorro [b], M.R. González [e], A. de Frutos [b]

[a] *Instituto de Agricultura Sostenible (IAS), Consejo Superior de Investigaciones Científicas (CSIC), Alameda del Obispo, s/n 14004-Córdoba, Spain*
[b] *GOA-UVA, Universidad de Valladolid, Spain*
[c] *Centro de Investigación y Tecnología Agroalimentaria de Aragón (CITA), Spain*
[d] *Department Earth and Space Science and Engineering, York University, Toronto, Canada*
[e] *Departamento de Producción Vegetal y Recursos Forestales, Universidad de Valladolid, Spain*

Received 11 June 2005; received in revised form 5 September 2005; accepted 7 September 2005

Abstract

Methods for chlorosis detection and physiological condition monitoring in *Vitis vinifera* L. through accurate chlorophyll a and b content (C_{ab}) estimation at leaf and canopy levels are presented in this manuscript. A total of 24 vineyards were identified for field and airborne data collection with the *Compact Airborne Spectrographic Imager* (CASI), the *Reflective Optics System Imaging Spectrometer* (ROSIS) and the *Digital Airborne Imaging Spectrometer* (DAIS-7915) hyperspectral sensors in 2002 and 2003 in northern Spain, comprising 103 study areas of 10×10 m in size, with a total of 1467 leaves collected for determination of pigment concentration. A subsample of 605 leaves was used for measuring the optical properties of reflectance and transmittance with a Li-Cor 1800-12 Integrating Sphere coupled by a 200 μm diameter single mode fiber to an Ocean Optics model USB2000 spectrometer. Several narrow-band vegetation indices were calculated from leaf reflectance spectra, and the PROSPECT leaf optical model was used for inversion using the extensive database of leaf optical properties. Results showed that the best indicators for chlorophyll content estimation in *V. vinifera* L. leaves were narrow-band hyperspectral indices calculated in the 700–750 nm spectral region (r^2 ranging between 0.8 and 0.9), with poor performance of traditional indices such as the *Normalized Difference Vegetation Index* (NDVI). Results for other biochemicals indicated that the *Structure Insensitive Pigment Index* (SIPI) and the *Photochemical Reflectance Index* (PRI) were more sensitive to carotenoids C_{x+c} and chlorophyll–carotenoid ratios C_{ab}/C_{x+c} than to chlorophyll content C_{ab}. Chlorophyll *a* and *b* estimation by inversion of the PROSPECT leaf model on *V. vinifera* L. spectra was successful, yielding a determination coefficient of $r^2 = 0.95$, with an RMSE = 5.3 μg/cm^2. The validity of leaf-level indices for chlorophyll content estimation at the canopy level in *V. vinifera* L. was studied using the *scaling-up* approach that links PROSPECT and rowMCRM canopy reflectance simulation to account for the effects of vineyard structure, vine dimensions, row orientation and soil and shadow effects on the canopy reflectance. The index calculated as a combination of the *Transformed Chlorophyll Absorption in Reflectance Index* (TCARI), and the *Optimized Soil-Adjusted Vegetation Index* (OSAVI) in the form TCARI/OSAVI was the most consistent index for estimating C_{ab} on aggregated and pure vine pixels extracted from 1 m CASI and ROSIS hyperspectral imagery. Predictive relationships were developed with PROSPECT–rowMCRM model between C_{ab} and TCARI/OSAVI as function of LAI, using field-measured vine dimensions and image-extracted soil background, row-orientation and viewing geometry values. Prediction relationships for C_{ab} content with TCARI/OSAVI were successfully applied to the 103 study sites imaged on 24 fields by ROSIS and CASI airborne sensors, yielding $r^2 = 0.67$ and RMSE = 11.5 μg/cm^2.

Keywords: Hyperspectral remote sensing; *Vitis vinifera*; Vineyards; Vine; Radiative transfer; Scaling-up; Optical index; RowMCRM

1. Introduction

Current research efforts in precision viticulture and on the temporal and spatial monitoring of *Vitis vinifera* L. show a growing interest in remote sensing methods due to its potential

* Corresponding author. Tel.: +34 957 499 280/+34 676 954 937; fax: +34 957 499 252.
E-mail address: pzarco@ias.csic.es (P.J. Zarco-Tejada).
URL: http://www.ias.csic.es/pzarco (P.J. Zarco-Tejada).

0034-4257/$ - see front matter © 2005 Elsevier Inc. All rights reserved.
doi:10.1016/j.rse.2005.09.002

for estimating vine biophysical variables such as shape, size and vigor, potential indicators of fruit quality and yield (a full review of optical remote sensing methods for vineyard monitoring can be found in Hall et al., 2002).

Successful mapping of vineyard leaf area index (LAI) using high spatial IKONOS satellite imagery was shown by Johnson et al. (2003), enabling the monitoring of plant growth for irrigation support and canopy management through temporal relationships between *Normalized Difference Vegetation Index* (NDVI) and Leaf Area Index (LAI) (Johnson, 2003). This index and other ratios were tested by Dobrowski et al. (2002; 2003) such as the *Perpendicular Vegetation Index* (PVI) and the *Ratio Vegetation Index* (RVI) derived from field data and multispectral aerial photography to estimate canopy density and dormant pruning weight prediction, suggesting consistency across growing seasons. As a result of these and other studies, broad-band multispectral remote sensing imagery of high spatial resolution shows potential applications for vineyard canopy structure characterization, leading to a successful estimation of vine canopy size, shape and row identification (Hall et al., 2003), vineyard mortality detection and missing vinestock recognition (Lagacherie et al., 2001), vineyard classification methods (Lanjeri et al., 2001), and vine canopy cover estimation for water management (Montero et al., 1999). These studies point toward the application of new techniques in viticulture based on precision agriculture, introducing methods focused on describing homogeneous management zones derived from remotely sensed biophysical variable estimates (Hall et al., 2002), connecting the within-field variability and the suggested classification of the field into different vigor classes with a potential wine quality production (Johnson et al., 2001).

Nevertheless, and despite the cited work conducted mainly with aerial photography, analogue camera systems, and digital sensors with a limited number of broad bands, little progress has been made on the remote sensing detection of vineyard physiology and condition due to the specific characteristics of the sensors needed, requiring simultaneous narrow-band capabilities and high spatial resolution. Progress on crop condition in vineyards has been made at the leaf-level studying absorptance in the visible region in the field (Schultz, 1996), and detecting phenology and grape color at harvest to gather information about berry phenolics (Lamb et al., 2004). For this reason, and due to such limited work achieved on the remote sensing of vine physiology and condition at canopy level, current research efforts are warranted toward the investigation of physical methods applied to high-spatial resolution hyperspectral remote sensing imagery to estimate leaf biochemical constituents and canopy biophysical variables to gather information related to vine status and functioning (Zarco-Tejada et al., 2003). Several studies indicate that the estimation of leaf biochemistry may be used as indicators of chlorosis due to plant stress and nutritional deficiencies caused by micro and macro elements (Fernandez-Escobar et al., 1999; Jolley & Brown, 1994; Marschner et al., 1986; Tagliavini & Rombolà, 2001; Wallace, 1991). As an example, element deficiencies such as iron and nitrogen may result in vine chlorosis and may cause a decrease of fruit yield and quality in the current and the subsequent year as fruit buds develop poorly (Tagliavini & Rombolà, 2001).

Leaf biochemistries, such as the concentration of chlorophyll a+b (C_{ab}), water (C_w), and dry matter (C_m), are indicators of stress and growth that may be estimated by empirical methods (indices) and analytical techniques (physical methods) from remote sensing data in the 400–2500 nm spectral region. Several studies demonstrate the feasibility of chlorosis detection in vegetation through C_{ab} estimation using spectroscopy and leaf optical properties (Carter & Spiering, 2002; Gitelson et al., 2003; Jacquemoud et al., 1996; le Maire et al., 2004; Sims & Gamon, 2002). Recently, several new optical indices have been proposed to relate crop physiological status with hyperspectral data through their relationship to biochemical constituent concentrations such as chlorophyll (Carter, 1994; Gitelson & Merzlyak, 1996; Vogelmann et al., 1993; Zarco-Tejada et al., 2001, 2004, 2005), carotenoids (Fuentes et al., 2001; Sims & Gamon, 2002), and water content (Gao, 1996; Peñuelas et al., 1997).

A large number of the new narrow-band optical indices that might be used with leaf and canopy hyperspectral reflectance have been tested on specific crop and forest species with success (Haboudane et al., 2002, 2004; Zarco-Tejada et al., 2001; a full review of indices can be found in Zarco-Tejada et al., 2005). Red edge reflectance indices, spectral and derivative indices, and derivative ratios have demonstrated good results for C_{ab} estimation from canopy reflectance using airborne hyperspectral data. Recently, combinations of indices based on the *Transformed Chlorophyll Absorption in Reflectance Index*, TCARI (Haboudane et al., 2002), *Modified Chlorophyll Absorption in Reflectance* MCARI (Daughtry et al., 2000), and the *Optimized Soil-Adjusted Vegetation Index*, OSAVI (Rondeaux et al., 1996), such as TCARI/OSAVI and MCARI/OSAVI, have been demonstrated to successfully minimize soil background and LAI variation in crops, providing predictive relationships for precision agriculture applications with hyperspectral imagery in closed crops (Haboudane et al., 2002) and open tree canopy orchards (Zarco-Tejada et al., 2004). Nevertheless, and despite the successful relationships obtained between specific optical indices and leaf biochemistry in closed crops, estimation of such biochemical components in vineyards at a canopy level from remote sensing requires appropriate modeling strategies accounting for its row-structure and large shadow and soil effects on the *bi-directional* reflectance (BRDF) signature. The application of previously validated leaf optical indices to discontinuous crop canopies such as *V. vinifera* L. needs extensive research with airborne hyperspectral data of optimum spatial and spectral resolution, i.e. one meter or better spatial resolution to obtain pure vine reflectance in selected spectral bands sensitive to pigment absorption. Vine row geometry leads to large variations in shadow scene proportions as a function of sun azimuth and zenith angles relative to row orientation, affecting the vegetation index and the estimated leaf biochemical constituent. It is required, therefore, that successful vine leaf-level indices are investigated at the canopy level through *scaling-up* simulation using

appropriate physical methods and very high spatial resolution. This approach (Haboudane et al., 2002; Zarco-Tejada et al., 2001, 2003) uses physical models at leaf and canopy levels to *scale-up* optical indices that are sensitive to specific biochemical constituents, therefore modeling the indices as function of canopy structure, viewing geometry and background effects.

This manuscript reports on a study of the optical properties of *V. vinifera* L. for C_{ab} estimation using narrow-band indices and radiative transfer model inversion. The work describes in detail the methods for accurate measurements of the leaf optical properties, testing the behavior of several indices for successful C_{ab} estimation. The successful leaf optical indices are proposed for *scaling-up* simulation with the *Markov-Chain Canopy Reflectance Model* (MCRM) (Kuusk, 1995a,b) with additions to simulate the row crop structure, called rowMCRM, and developed within the frame of the *Crop Reflectance Operational Models for Agriculture* (CROMA) project. The linked PROSPECT–rowMCRM model is assessed to model vineyard scene component proportions, row orientations, vineyard dimensions and background effects with high spatial resolution hyperspectral airborne imagery.

2. Airborne and field campaigns for data collection

2.1. Airborne campaigns with ROSIS and CASI hyperspectral sensors

Data acquisition campaigns were conducted in July 2002 under the European Union HySens-2002 project intended to investigate physical methods with the *Reflective Optics System Imaging Spectrometer* (ROSIS) and the *Digital Airborne Imaging Spectrometer* (DAIS-7915) airborne hyperspectral sensors to estimate leaf biochemical constituents in vineyard canopies. In July 2003 the *Compact Airborne Spectrographic Imager* (CASI) sensor was flown over Spain in collaborative research with York University (Canada) and the Spanish aerospace institute *Instituto Nacional de Técnica Aeroespacial* (INTA). Both campaigns took place in study areas of *V. vinifera* L. in *Ribera del Duero* D.O. in Northern Spain.

ROSIS imagery were acquired at 1 m spatial resolution, and calibrated to *at-sensor* radiance by the *German Aerospace Center* (DLR). CASI imagery were collected on two airborne missions, each with a specific sensor mode of operation: i) the *Mapping Mission*, with 1 m spatial resolution and 8 *user-selected* spectral bands placed in the spectrum to enable the calculation of specific narrow-band indices sensitive to pigment concentration (bands were centered at 490, 550, 670, 700, 750, 762, 775 and 800 nm with *full-width at half maximum* (FWHM) ranging between 7 and 12 nm); and the *Hyperspectral Mission*, with 4 m spatial resolution, 72 channels and 7.5 nm spectral resolution. The 12-bit radiometric resolution data collected by CASI were processed to *at-sensor* radiance using calibration coefficients derived in the laboratory by the Earth Observations Laboratory (EOL), York University, Canada. Aerosol optical depth data at 340, 380, 440, 500, 670, 870, and 1020 nm were collected using a Micro-Tops II sunphotometer (Solar Light Co., Philadelphia, PA, USA) in the study area at the time of data acquisition to derive aerosol optical depth at 550 nm. Atmospheric correction was applied to ROSIS radiance imagery using MODTRAN, whereas the CAM5S atmospheric correction model (O'Neill et al., 1997) was used for CASI imagery. Reflectance data were geo-referenced using GPS data collected onboard the aircraft. Soil reflectance spectra were used to perform a *flat-field* correction (Ben-Dor & Levin, 2000) that compensated for residual effects on derived surface reflectance estimations in atmospheric water and oxygen absorption spectral regions. Fig. 1 shows vegetation and soil spectra extracted from CASI mapping mission image on selected sites after processing to *surface reflectance*, observing the large variability in soil brightness levels, as well as the pure vine and the mixed soil+vine+shadow spectra.

Concurrent with the airborne overflights, field sampling campaigns were conducted in summer 2002 and 2003 for biochemical analysis of leaf C_{ab}, as well as to measure reflectance (R) and transmittance (T) from leaf samples to study the vine optical properties.

2.2. Study site description and leaf sampling methods

The study sites of *V. vinifera* L. used for ground and airborne collection were carefully selected from a plot network currently monitored by the local government to assure a gradient in the leaf biochemistry as sought for this study. A total of 10 fields were selected in 2002 and 14 fields in 2003 for leaf sampling collection, comprising a total of 103 study areas of 10×10 m in size. In 2002, 10 leaves per site were used for Cab sampling and reflectance and transmittance measurements. In 2003, a total of 80 leaves were sampled from each 10×10 m study area, using 50 leaves for measuring dry matter and elements N, P, K, Ca, Mg, Fe, 20 leaves for Cab determination, and 10 leaves per site for conducting reflectance and transmittance measurements. A total of 1467 leaves were used for determination of Cab on the 103 study sites comprised by the 2002 and 2003 campaigns, and 605 leaves for measuring the optical properties. Leaves used for measuring optical properties were taken to the laboratory and reflectance and transmittance measurements made on the same day to avoid pigment degradation. Dry matter was measured placing the samples in a pre-heated oven at 40 °C until a stable dry weight was reached. Structural measurements on each study site consisted of grid size, number of vines within the 10×10 m site, trunk height, vegetation height and width, and row orientation. Soil samples were collected at each site for laboratory analysis. Fig. 2 illustrates a CASI image acquired from vineyard fields, showing 15 out of the total 103 blocks of 10×10 m used for leaf sampling and ground data collection.

2.3. Leaf pigment determination by destructive sampling

The leaves from the *V. vinifera* L. sites were sampled from the top of the canopy, eliminating the small leaves indicative of low expansion. Leaves were placed in paper bags to allow tissue respiration and conservation, then stored at 4 °C prior to

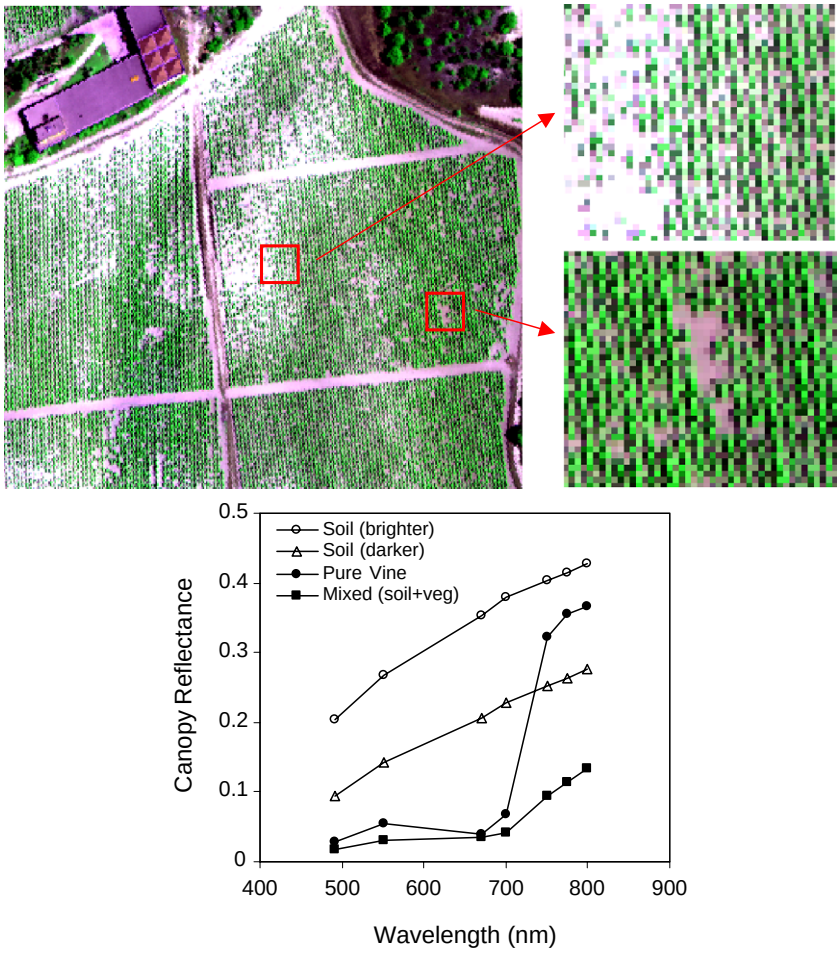

Fig. 1. Airborne CASI image collected at 1 m spatial resolution and 8 bands selected for calculation of narrow-band indices sensitive to pigment concentration. Pure vine reflectance and soil spectra extracted from the image show the within-field variability.

analysis of reflectance and transmittance, and then stored in a freezer at −8 °C prior to pigment determination. A 1.6 cm circle from each leaf sample was cut out for grinding with 4 ml acetone at 80%, and adding 8 ml acetone to a total of 12 ml in each tube. Tubes were stored in the dark at 4 °C for 48 h prior to spectrophotometer measurements. Each sample for pigment determination was filtered, placed in a cuvette and the absorbance measured between 400 and 700 nm with 2 nm fixed resolution at 1 nm interval with a Jasco V-530 UV-VIS spectrophotometer (Jasco Inc., Great Dunmow, UK). Chloro-

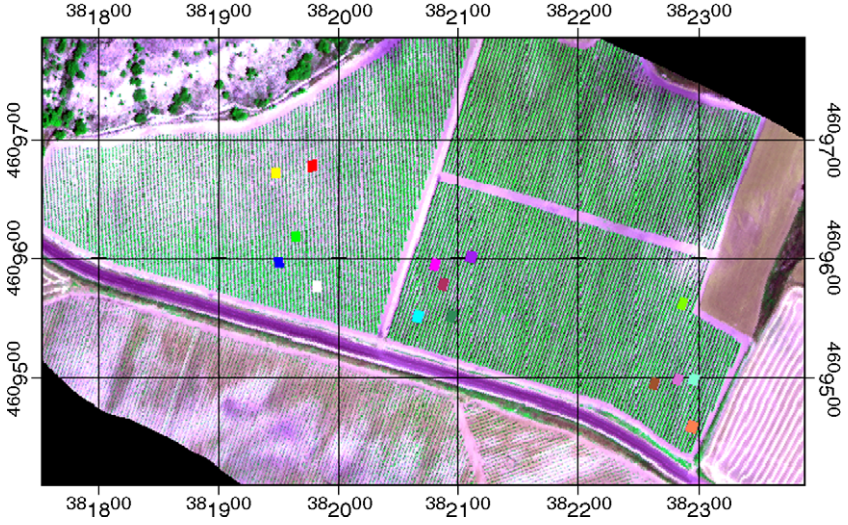

Fig. 2. Airborne hyperspectral CASI image acquired from one of the *Vitis vinifera* L. fields in this study, showing 15 blocks of 10 × 10 m selected for leaf sampling and ground data collection.

Table 1
Range of variation for the leaves sampled from the 103 study sites of *Vitis vinifera* L. used in this study

	C_a	C_b	C_{ab}	C_{x+c}	C_a/C_b	C_a/C_{x+c}	C_b/C_{x+c}	C_{ab}/C_{x+c}
Max	54.03	19.87	73.45	13.98	4.29	5.08	1.77	6.75
Min	1.74	1.25	3.40	1.39	1.05	0.74	0.33	1.06
Average	26.01	8.98	34.99	7.90	2.92	3.20	1.11	4.31

Values in μg/cm^2 (n=1467).

phyll *a* (C_a), chlorophyll *b* (C_b), and total carotenoid (C_{x+c}) concentrations were calculated using the extinction coefficients derived by Wellburn (1994) and the absorbance measured at 470, 646, and 663 nm with Eqs. (1)–(3).

$$C_a = 12.21 \cdot A_{663} - 2.81 \cdot A_{646} \quad (1)$$

$$C_b = 20.13 \cdot A_{646} - 5.03 \cdot A_{663} \quad (2)$$

$$C_{x+c} = (1000 \cdot A_{470} - 3.27 \cdot C_a - 104 \cdot C_b)/198. \quad (3)$$

These measurements resulted in a mean C_{ab} of μ=34.99 μg/cm^2, with a wide range between 3.4 and 73.45 μg/cm^2 (n=1467). Table 1 shows the range of variation of C_a, C_b, C_{ab} and C_{x+c} used later for determination of pigment content at each study site. The range of variation of the subset of 605 leaves used for optical measurements, correlation with optical indices and modelling are shown in Table 2.

2.4. Protocol for optical measurements of V. vinifera L. leaves

Reflectance and transmittance measurements of vine leaves were conducted on the subsample of 605 leaves with a Li-Cor 1800-12 Integrating Sphere (Li-Cor, Inc., Lincoln, NE, USA), coupled by a 200 μm diameter single mode fiber to an Ocean Optics model USB2000 spectrometer (Ocean Optics Inc., Dunedin, FL, USA), with a 2048 element detector array, 0.5 nm sampling interval, and 7.3 nm spectral resolution in the 350–1000 nm range. Software was designed for signal verification, adjustment of integration time, and data acquisition. An integration time of 13 ms was used for all sample measurements. Spectral bandpass characterization performed using a mercury spectral line lamp source yielded FWHM bandwidth estimates of 7.3 at 546.1 nm. Fiber spectrometer wavelength calibration was performed using the Ocean Optics HG-1 Mercury–Argon Calibration Source that produces Hg and Ar emission lines between 253 and 922 nm. Single leaf reflectance and transmittance measurements were acquired following the methodology described in the manual for the Li-Cor 1800-12 system (Li-Cor Inc., 1984) modified by Harron (2000) to correct for stray-light in the integrating sphere. For clarity, the protocol is described here with the steps required to calculate the stray-light corrected leaf hemispherical reflectance (R) and transmittance (T) using a reference target in the integrating sphere. The protocol consisted of a total of five measurements modifying the position of the collimated light, dark and white plugs in the integrating sphere to measure the transmittance signal (TSP), the reflectance signal (RSS), the reflectance internal standard (RTS), the reflectance ambient (RSA), and the dark measurement (DRK) (Table 3)). For clarity of the protocol used in this study and for future reference, a schematic view of the integrating sphere with lamp and port placement is shown in Fig. 3. Stray-light corrected reflectance and transmittance were then calculated assuming a constant center wavelength and spectral bandpass, using the set of equations described by Harron (2000) for stray-light correction in broadleaves without the requirement of sample carriers (Eqs. (4)–(8)). Another measurement protocol and a different set of equations are proposed in Harron (2000) when measuring needle samples or broad leaves smaller than the sphere sample port.

$$R = R' \frac{GT_{fi} + \frac{R'}{R_{BaSO_4}} S_i R_w T_f}{GT_{fi} + S_i R_w T_f} \quad (4)$$

$$T = T' \left(1 + \frac{S_i R_w R T_f}{GT_{fi} R_{BaSO_4}}\right) \quad (5)$$

with R', $T'$and G given in Eqs. (6), (7) and (8),

$$R' = \frac{RSS - RSA}{RTS - RSA} R_{BaSO_4} \quad (6)$$

$$T' = \frac{TSP - DRK}{RTS - RSA} R_{BaSO_4} \quad (7)$$

$$G = (1 - W_f R_w - B_f R_{BaSO_4}) \quad (8)$$

with the following coefficients measured for the sphere used in this study,

W_f is the fraction of the sphere which is interior wall (0.968)
B_f is the fraction of the sphere which is $BaSO_4$ reference (0.009)

Table 2
Range of variation for the subsample of *Vitis vinifera* L. leaves used for optical measurements and correlations with optical indices

	C_a	C_b	C_{ab}	C_{x+c}	C_a/C_b	C_a/C_{x+c}	C_b/C_{x+c}	C_{ab}/C_{x+c}
Max	53.79	19.49	70.83	13.98	4.29	4.31	1.67	5.98
Min	1.74	1.25	3.40	1.39	1.05	0.96	0.35	1.50
Average	25.43	8.80	34.23	7.99	2.91	3.09	1.08	4.17

Values in μg/cm^2 (n=605).

Table 3
Sequence of measurements with the Li-Cor 1800 integrating sphere and fiber spectrometer to enable the calculation of reflectance and transmittance with Eqs. (4)–(8) and the schematic view shown in Fig. 3

Step	Setup	Lamp	White plug	Dark plug	Sample
1	RSA	C (ON)	B	A	OUT
2	RSS	C (ON)	B	A	IN←
3	RTS	B (ON)	C	A	IN←
4	TSP	A (ON)	C	B	IN→
5	DRK	OFF	B	A	OUT

IN →: adaxial leaf surface facing sample port A.
IN ←: adaxial leaf surface facing sphere.

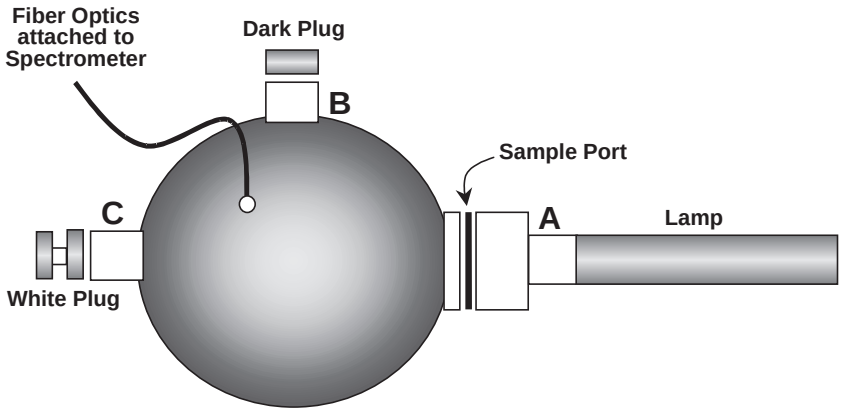

Fig. 3. Schematic view of the Li-Cor 1800-12 integrating sphere attached to an USB2000 fiber spectrometer used for reflectance and transmittance measurements.

T_{fi} is the fraction of the sphere which is target and directly illuminated (0.006)
T_f is the fraction of the sphere which is target (0.009)
S_i is the fraction of light scattered into the sphere from the illuminator (0.0001)
R_{BaSO_4} is the reflectance of the $BaSO_4$ reference (0.98)
R_w is the reflectance of sphere walls (0.9).

Experimental measurements made with the Li-Cor 1800-12 integrating sphere used in this study were employed to calculate the fraction of light scattered into the sphere from the illuminator (S_i), a function of the optical properties of the sphere and light lamp used. The S_i value obtained for the sphere used in this study was 10^{-4}, indicating that such correction factor had a very small effect on the calculated reflectance and transmittance. Nevertheless, on another integrating sphere used on this same study with different design and configuration (data not shown), the S_i correction was critical for an accurate calculation of the leaf optical properties corrected for stray-light, and therefore it has to be seriously taken into consideration in such cases. As an example of spectra measured with this methodology, Fig. 4 shows vine leaf reflectance and transmittance spectra with pigment content of 26.68 μg/cm^2, and 4 leaf reflectance measurements from leaves containing a gradient in chlorophyll concentration between 15 and 54 μg/cm^2.

3. Vegetation indices and model inversion for C_{ab} estimation in *V. vinifera* L. at the leaf-level

Leaf-level spectroscopy enables the calculation of narrow-band indices potentially related to specific light absorptions caused by leaf biochemical constituents, such as chlorophyll *a* and *b* (Carter & Spiering, 2002; Sims & Gamon, 2002; Zarco-Tejada et al., 2005), carotenoids/chlorophyll and anthocyanins/chlorophyll ratios (Fuentes et al., 2001; Gamon & Surfus, 1999; Peñuelas et al., 1995), dry matter (Fourty & Baret, 1997), and water content (Carter, 1991; Ceccato et al., 2001; Danson et al., 1992; Gao, 1996; Peñuelas et al., 1997). Several optical indices are currently used with success for C_{ab} estimation from leaf optical properties on different crop and forest species, exploiting the differences in reflectance between healthy and stressed vegetation in the visible and the red edge spectral region (Carter, 1994; Carter & Spiering, 2002; Horler et al., 1983; Vogelmann et al., 1993; Zarco-Tejada et al., 2001). A full review of these chlorophyll indices can be found in Zarco-Tejada et al. (2001, 2004, 2005) and summarized in Table 4. These indices are generally classified into visible and visible/NIR ratios, red edge indices and spectral and derivative

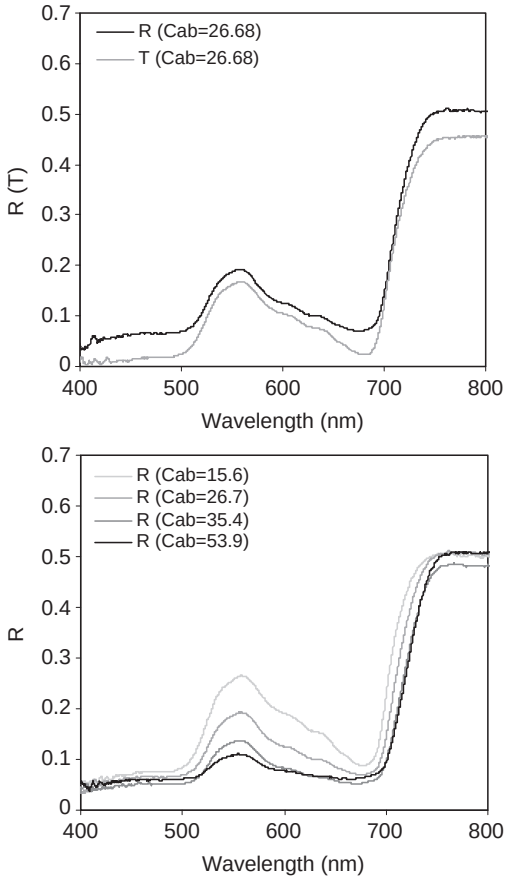

Fig. 4. Sample leaf reflectance (R) and transmittance (T) measured in a *Vitis vinifera* L. leaf with integrating sphere and protocol described in this manuscript. Destructive C_{ab} determination yielded a chlorophyll content of 26.68 μg/cm^2 (upper plot). Bottom plot shows 4 leaf reflectance measurements for vine leaves containing 15.6, 26.7, 35.4, and 53.9 μg/cm^2 respectively.

Table 4
Hyperspectral optical indices used in this study

Vegetation index	Equation	Reference
Normalized Difference Vegetation Index (NDVI)	$NDVI = (R_{NIR} - R_{red})/(R_{NIR} + R_{red})$	Rouse et al. (1974)
Simple Ratio Index (SR)	$SR = R_{NIR}/R_{red}$	Jordan (1969); Rouse et al. (1974)
Modified Simple Ratio (MSR)	$MSR = \frac{R_{NIR}/R_{red} - 1}{(R_{NIR}/R_{red})^{0.5} + 1}$	Chen (1996)
Modified Triangular Vegetation Index ($MTVI_1$)	$MTVI_1 = 1.2*[1.2*(R_{800} - R_{550}) - 2.5*(R_{670} - R_{550})]$	Haboudane et al. (2004)
Modified Triangular Vegetation Index ($MTVI_2$)	$MTVI_2 = \frac{1.5*[1.2*(R_{800} - R_{550}) - 2.5*(R_{670} - R_{550})]}{\sqrt{(2*R_{800} + 1)^2 - (6*R_{800} - 5*\sqrt{R_{670}}) - 0.5}}$	Haboudane et al. (2004)
Renormalized Difference Vegetation Index (RDVI)	$RDVI = (R_{800} - R_{670})/\sqrt{(R_{800} + R_{670})}$	Rougean and Breon (1995)
Greenness Index (G)	$G = R_{554}/R_{677}$	–
Triangular Veg. Index (TVI)	$TVI = 0.5*[120*(R_{750} - R_{550}) - 200*(R_{670} - R_{550})]$	Broge and Leblanc (2000)
Improved SAVI with self-adjustment factor L (MSAVI)	$MSAVI = \frac{1}{2}\left[2*R_{800} + 1 - \sqrt{(2*R_{800} + 1)^2 - 8*(R_{800} - R_{670})}\right]$	Qi et al. (1994)
Optimized Soil-Adjusted Vegetation Index (OSAVI)	$OSAVI = (1 + 0.16)*(R_{800} - R_{670})/(R_{800} + R_{670} + 0.16)$	Rondeaux et al. (1996)
Modified C_{ab} Absorption in Reflectance Index (MCARI)	$MCARI = [(R_{700} - R_{670}) - 0.2*(R_{700} - R_{550})]*(R_{700}/R_{670})$	Daughtry et al. (2000)
Transformed CARI (TCARI)	$TCARI = 3*[(R_{700} - R_{670}) - 0.2*(R_{700} - R_{550})*(R_{700}/R_{670})]$	Haboudane et al (2002)
Modified Chlorophyll Absorption in Reflectance Index ($MCARI_1$)	$MCARI_1 = 1.2*[2.5*(R_{800} - R_{670}) - 1.3*(R_{800} - R_{550})]$	Haboudane et al. (2004)
Modified Chlorophyll Absorption in Reflectance Index ($MCARI_2$)	$MCARI_2 = \frac{1.5*[2.5*(R_{800} - R_{670}) - 1.3*(R_{800} - R_{550})]}{\sqrt{(2*R_{800} + 1)^2 - (6*R_{800} - 5*\sqrt{R_{670}}) - 0.5}}$	Haboudane et al. (2004)
Zarco and Miller (ZM)	$ZM = R_{750}/R_{710}$	Zarco-Tejada et al. (2001)
Blue/Green and Blue/Red Pigment ndices (RGI, BGI, BRI)	$RGI = R_{690}/R_{550}$ $BGI_1 = R_{400}/R_{550}$ $BGI_2 = R_{450}/R_{550}$ $BRI_1 = R_{400}/R_{690}$ $BRI_2 = R_{450}/R_{690}$	Zarco-Tejada et al. (this study)
Simple Ratio Pigment Ind. (SRPI)	$SRPI = R_{430}/R_{680}$	Peñuelas et al. (1995)
Normalized Phaeophytinization Index (NPQI)	$NPQI = (R_{415} - R_{435})/(R_{415} + R_{435})$	Barnes (1992)
Photochemical Reflectance Index (PRI)	$PRI_1 = (R_{528} - R_{567})/(R_{528} + R_{567})$ $PRI_2 = (R_{531} - R_{570})/(R_{531} + R_{570})$ $PRI_3 = (R_{570} - R_{539})/(R_{570} + R_{539})$	Gamon et al. (1992)
Normalized Pigment Chlorophyll Index (NPCI)	$NPCI = (R_{680} - R_{430})/(R_{680} + R_{430})$	Peñuelas et al. (1994)
Carter Indices (CTR)	$CTR_1 = R_{695}/R_{420}$ $CTR_2 = R_{695}/R_{760}$	Carter (1994,1996)
Lichtenthaler Indices (LIC)	$LIC_1 = (R_{800} - R_{680})/(R_{800} + R_{680})$ $LIC_2 = R_{440}/R_{690}$ $LIC_3 = R_{440}/R_{740}$	Lichtenthaler et al. (1996)
Structure Insensitive Pigment Index (SIPI)	$SIPI = (R_{800} - R_{450})/(R_{800} + R_{650})$	Peñuelas et al. (1995)
Vogelmann Indices (VOG)	$VOG_1 = R_{740}/R_{720}$ $VOG_2 = (R_{734} - R_{747})/(R_{715} + R_{726})$ $VOG_3 = (R_{734} - R_{747})/(R_{715} + R_{720})$	Vogelmann et al. (1993); Zarco-Tejada et al. (2001)
Gitelson and Merzlyak (GM)	$GM_1 = R_{750}/R_{550}$ $GM_2 = R_{750}/R_{700}$	Gitelson and Merzlyak (1997)
Curvature Index (CUR)	$CUR = (R_{675} \cdot R_{690})/(R_{683}^2)$	Zarco-Tejada et al. (2000)

analysis indices. Other traditional indices related to vegetation structure and condition, such as NDVI or the Simple Ratio (SR), normally show low relationships with leaf biochemical constituents (Zarco-Tejada et al., 2001) and consistently show unsuccessful performance in detecting physiological stress condition.

Despite the demonstrated success of these narrow-band leaf indices for C_{ab} estimation, spectral reflectance signatures from agricultural canopies are characterized by large contributions from the soil background and LAI variation at different growth stages. In these cases, *scaling-up* methods through canopy reflectance models are needed to account for crop structure, viewing geometry and soil and shadow effects on the reflectance. The study of indices at both leaf and canopy levels demonstrates that successful indices developed at the leaf-level do not necessarily perform well at the canopy level due to the soil and structural effects mentioned (Zarco-Tejada et al., 2001, 2004). Therefore, combined indices have been proposed to minimize background soil effects while maximizing the sensitivity to C_{ab} (Haboudane et al., 2002) and LAI

(Haboudane et al., 2004) and to yield prediction relationships directly applicable to hyperspectral imagery. As an example, CARI *(Chlorophyll Absorption in Reflectance Index)* (Kim et al., 1994) was shown to reduce the variability induced on photosynthetically active radiation inferences due to non-photosynthetic materials. MCARI *(Modified Chlorophyll Absorption in Reflectance Index)* (Daughtry et al., 2000) was a modification of CARI to minimize the combined effects of the soil reflectance and the non-photosynthetic materials. SAVI *(Soil-Adjusted Vegetation Index)* (Huete, 1988) and OSAVI *(Optimized Soil-Adjusted Vegetation Index)* (Rondeaux et al., 1996) were proposed as soil-line vegetation indices that could be combined with MCARI to reduce background reflectance contributions (Daughtry et al., 2000). As a result of the development of these indices, successful C_{ab} estimation on corn agricultural canopies at different growing stages was achieved using the TCARI/OSAVI combined index in forward leaf-canopy modelling, proving its robustness due to the low sensitivity to effects caused by LAI variation and background influence (Haboudane et al., 2002). Other indices, such as the modified chlorophyll absorption ratio index (MCARI2), are discussed in depth in Haboudane et al. (2004). All these mentioned indices that can be found in Table 4 have proven different degrees of success in crop and forest species for pigment estimation at the leaf-level. Relationships between all these single and combined indices calculated from the 605 leaf R and T measurements in 2002 and 2003 campaigns (Table 4) and pigment content measurements C_a, C_b, C_{ab}, C_{x+c}, and pigment ratios C_a/C_b, C_a/C_{x+c}, C_b/C_{x+c} and C_{ab}/C_{x+c} (Table 2) were calculated using linear, exponential, and 3rd order polynomial functions to allow for both linear and non-linear relationships between indices and leaf pigment concentrations in grape leaves. The large database available of leaf optical measurements as part of this study addresses the lack of previous studies on investigating appropriate leaf optical indices in *V. vinifera* L. crop.

In addition to the generally accepted relationships existing between leaf optical indices and C_{ab}, model inversion methods using radiative transfer simulation have been successfully used to simulate leaf optical properties. Due to its extensive validation, the PROSPECT model (Jacquemoud & Baret, 1990), based on the *plate model* (Allen et al., 1969, 1970), was used in this study to simulate the leaf optical properties of *V. vinifera* L. leaves, testing the feasibility of C_{ab} estimation. Several studies demonstrate successful retrievals of pigment concentration from leaf optical properties with PROSPECT (Jacquemoud & Baret, 1990; Jacquemoud et al., 1996; le Maire et al., 2004) although limited simulation work has been conducted with extensive measurements on *V. vinifera* L leaves. The large database of leaf reflectance and transmittance spectra measured in 2002 and 2003, comprising a total of 605 measurements, were used for PROSPECT model inversion. The model inversion was performed by iterative optimization, varying input parameters N (structural parameter) from 1 to 2.5, C_{ab} between 5 and 95 μg/cm^2, C_m in the range 0.001 and 0.04 mg/cm^2, and C_w for 0.001 and 0.04 mg/cm^2, obtaining the root mean square error (RMSE) function $\xi(N)$ to be minimized using both R and T in the 400–800 nm range using Eq. (9),

$$\mathrm{RMSE} = \xi(N, C_{ab}, C_m, C_w) = \sqrt{\frac{\sum_{\lambda}\left[(R_{\mathrm{PROSPECT}} - R_m)_{\lambda}^2 + (T_{\mathrm{PROSPECT}} - T_m)_{\lambda}^2\right]}{n}} \quad (9)$$

where R_m and T_m are reflectance R and transmittance T measured from n leaf samples with the Li-Cor integrating sphere and fiber spectrometer. Estimated C_{ab} values from each R and T spectra by inversion were then compared with leaf destructive measurements of pigment concentration, and the RMSE for C_{ab} estimation from the entire database was calculated.

4. Application of leaf-level hyperspectral indices at canopy level in *V. vinifera* L. with the rowMCRM model

PROSPECT was linked to the rowMCRM model, which refers to the *Markov-Chain Canopy Reflectance Model* (MCRM) (Kuusk, 1995a,b) with additions to simulate the row crop structure. The rowMCRM model was developed within the frame of the *Crop Reflectance Operational Models*

Table 5
Nominal values and range of parameters used for leaf and canopy simulation with PROSPECT and rowMCRM for the vine study sites

PROSPECT	
Leaf parameters	Nominal values and range
Chlorophyll a+b (C_{ab})	5–95 μg/cm^2
Dry matter (C_m)	0.0035 mg/cm^2
Equivalent water thickness (C_w)	0.025 mg/cm^2
Structural parameter (N)	1.62
rowMCRM	
Canopy layer and structure parameters	Nominal values and range
Row Leaf Area Index (LAI)	1–5
Leaf Angle Distribution Function (LADF)	ε=0.95; θ_n=45° (plagiophile)
Relative leaf size (h_s)	0.083
Markov parameter (λ_z)	1.1
Leaf transmittance coefficient (t)	0.9
Leaf hair index (l_h)	0.1
Canopy height (C_H)	1.2–1.8 m
Crown width (C_W)	0.6–1.3 m
Visible soil strip length (V_s)	1.7–2.3 m
Diff. between sun azimuth and row direction (ψ)	11–95.2°
Background and viewing geometry	Nominal values and range
Soil reflectance (ρ_s)	From images (Fig. 7)
Angstrom turbidity factor (β)	0.18
Viewing geometry ($\theta_s\theta_v\ \phi$)	Calculated for each image and site

Canopy structural parameters were used in the rowMCRM model for simulation of the canopy reflectance by radiative transfer. Leaf structural parameters, and leaf biochemical parameters were used for leaf-level simulation of reflectance and transmittance using PROSPECT.

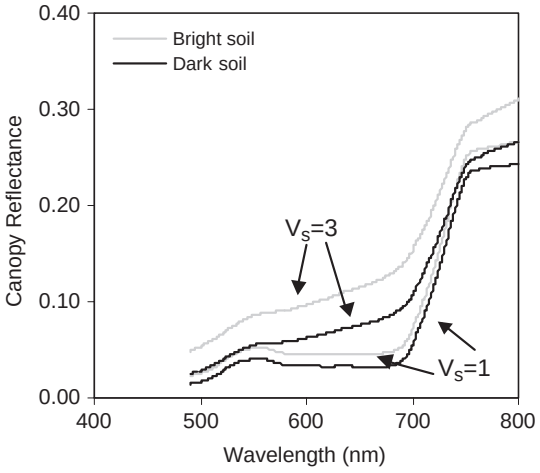

Fig. 5. Canopy reflectance simulation conducted with PROSPECT–rowMCRM as function of soil background (ρ_s) and visible soil strip (V_s).

for Agriculture project (CROMA), with a goal to successfully simulate different scene component proportions, as a function of row orientations and crop dimensions, and soil background and shadow effects as function of viewing geometry in *row-structured* crop canopies. Therefore the rowMCRM canopy reflectance model was considered an optimum candidate for the *scaling-up* of narrow-band indices in row-structured vineyard canopies. The inputs required to the link PROSPECT–rowMCRM used in this study are shown in Table 5: i) leaf parameters for simulating the leaf optical properties, such as chlorophyll a+b (C_{ab}), dry matter (C_m), water content (C_w), and structural parameter (N); ii) canopy layer and structure parameters such as the row leaf area index (LAI), leaf angle distribution function (LADF), relative leaf size (h_s), Markov parameter (λ_z), leaf transmittance coefficient (t), leaf hair index (l_h), canopy height (C_H), crown width (C_W), visible soil strip length (V_s), and the angular difference between sun azimuth and row direction (ψ); and iii) background and viewing geometry parameters such as soil reflectance (ρ_s), Angstrom turbidity factor (β), and the viewing geometry (θ_s, θ_v, ϕ).

Without an intention to provide an *in-depth* sensitivity analysis for rowMCRM (work conducted as part of CROMA project), an exploratory analysis was carried out to study the effects of the different input parameters for PROSPECT–rowMCRM on the canopy reflectance and selected optical indices. The soil background and distance between rows (visible soil strip) input for this row-structured canopy are shown to have large effects on the canopy reflectance (Fig. 5). As expected, soil brightness effects are greater as function of the visible soil strip, suggesting the importance of the vineyard architecture for successful simulation of the canopy reflectance. Typical vineyard canopies are planted in grids with a distance between rows of around 2 m (1.7 to 2.3 m range in the 103 study sites in this study), resulting in reflectance differences of

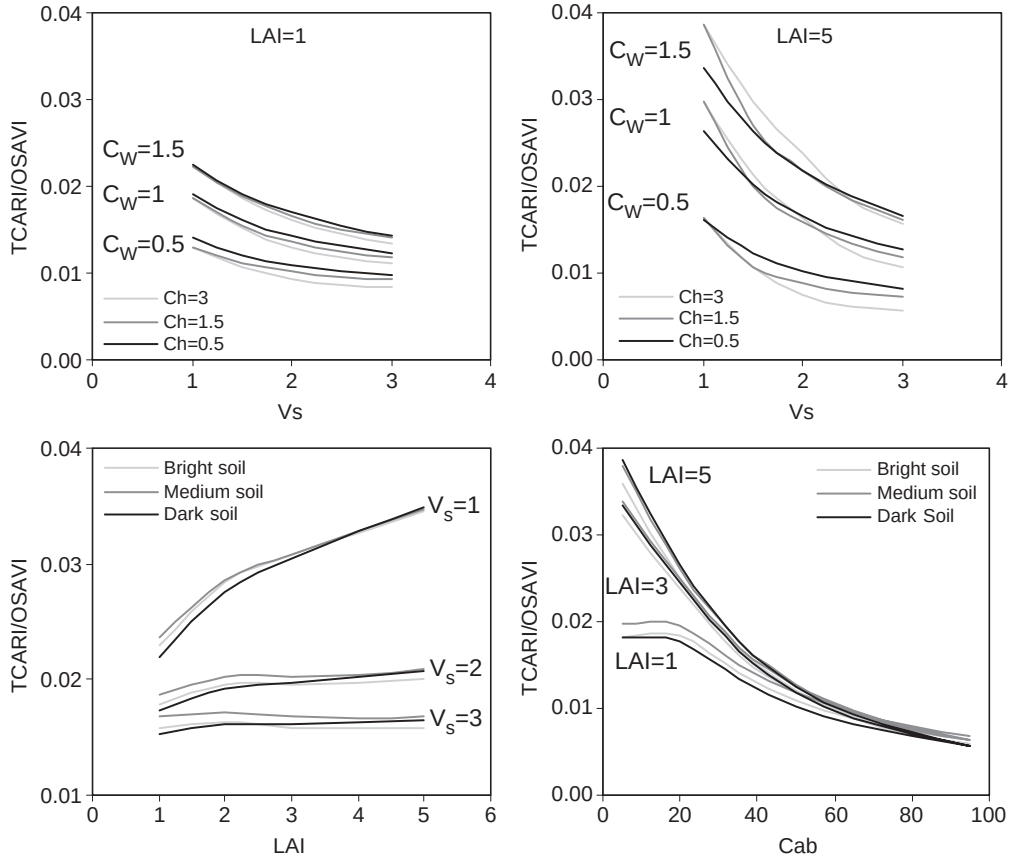

Fig. 6. Effects on TCARI/OSAVI for: i) vine width (C_w) and height (C_H) as function of visible soil strip (V_s) and row LAI (top left and right); ii) visible soil strip (V_s) as function of row LAI and soil background (ρ_s) (bottom left); and iii) row LAI and soil background (ρ_s) on TCARI/OSAVI as function of C_{ab} (bottom right).

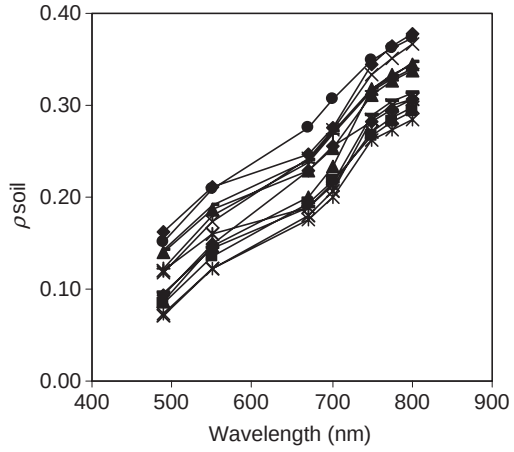

Fig. 7. CASI soil spectra extracted from vineyard study sites and used as input for the simulation methods.

5–7% at 700 nm as function of the soil brightness levels. The effects of row LAI, vineyard row width and height, visible soil strip, and chlorophyll content were then studied for the TCARI/OSAVI index, a combined ratio that has previously proven successful in minimizing background effects for C_{ab} retrieval. The study of vine width and height on TCARI/OSAVI as function of visible soil strip and row LAI (Fig. 6, top left and right) indicates that larger effects are expected due to vine width than to vine height, with larger effects on TCARI/OSAVI as LAI increases. As the visible soil strip increases, vine width effects decrease due to the greater contribution effects of soil reflectance, with lower contribution of vegetation. As LAI increases, large effects on TCARI/OSAVI are found when the visible soil strip is small, i.e. close to 1 m (Fig. 6, bottom left). Nevertheless, for visible soil strips greater than 1 m, i.e. 2 or 3 m (an average of 2 m in the vine sites of this study) simulations suggest a small effect of LAI variation. These simulations indicate that larger effects are found on the index as function of the visible soil strip (background effects) than due to the LAI variation, suggesting the importance for properly describing the vineyard architecture and soil characteristics. When LAI is greater than 1, i.e. 3 or 5 (Fig. 6, bottom right) simulation results suggest the low effects of LAI on TCARI/OSAVI as function of C_{ab} in vineyards with average dimensions (height = 1.5 m; width = 1 m; visible soil strip = 2 m). In addition, in low LAI and low C_{ab} sites (Fig. 6, bottom left and right) soil backgrounds are shown to be important, decreasing the effects on TCARI/OSAVI as row LAI and C_{ab} increase.

These simulations indicate the importance of properly describing the vineyard architecture and dimensions, and the soil background for accurate estimates of chlorophyll concentration. Therefore, in this study vineyard structural parameters and airborne-sun viewing geometry angles that varied between fields were taken into account as inputs for *scaling-up* methods with the rowMCRM canopy model for simulation on each one of the 103 study plots. Vineyard planting grids ranged between 2.5×1 and 3×1.5 m, vine height between 1.2 and 1.8 m, vine width between 0.6 and 1.3 m, visible soil strip between 1.7 and 2.3 m, difference between sun azimuth and row direction between 11° and 95°, and sun zenith angle between 31.5° and 46.7° for all images collected on the airborne campaigns for the 2 years and 103 sites. In addition, simulation methods for C_{ab} estimation employed the input of soil reflectance spectra obtained directly from the imagery on areas of canopy openings or missing vines within the field. Fig. 7 shows a range of soil spectra extracted from the CASI imagery from each of the 14 fields acquired in the 2003 campaign, illustrating the gradient in soil brightness and differences greater than 10% reflectance.

Predictive relationships were calculated for each field study site between C_{ab} and optical indices, using image and field-measured parameters for the vineyard structure, soil background and viewing geometry. *Scaling-up* methods used here are similar to the ones described in Zarco-Tejada et al. (2001) for forest canopies, Haboudane et al. (2002, 2004) for corn crops using PROSPECT-SAILH, and Zarco-Tejada et al. (2004) for open tree canopy crops using PROSPECT-SAILH-FLIM models. *Scaling-up* relationships were developed for each study site using a range of LAI values between 1 and 5, and between 5 and 95 μg/cm^2 for C_{ab}, fixing the remaining leaf

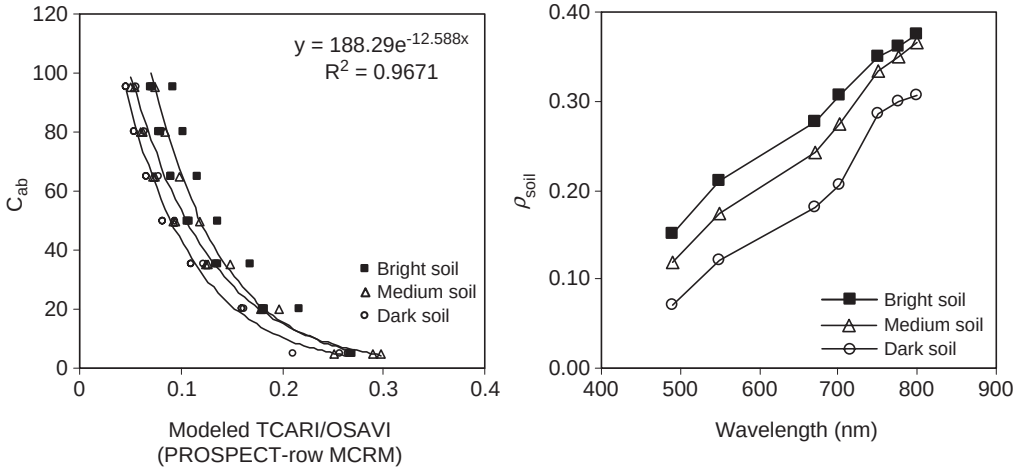

Fig. 8. Example of 3 predictive relationships (left) developed for study sites with extreme soil backgrounds (right). Relationships were developed using a range of row LAI values between 1 and 5, C_{ab} ranging between 5 and 95 μg/cm^2 and structural parameters measured in the field. The remaining parameters were fixed to the values shown in Table 5.

parameters to the values estimated by model inversion from the leaf samples previously described, with the field structural measurements describing the vineyard canopy structure on each study site (Table 5; Fig. 8). Estimated C_{ab} for each of the 103 study sites was then compared with the field-measured values of pigment content obtained by destructive sampling and described in the previous section.

5. Results

Analysis conducted on the 605 leaves where optical properties and leaf biochemical constituents C_a, C_b, C_{ab}, C_{x+c} and ratios C_a/C_b, C_a/C_{x+c}, C_b/C_{x+c}, C_{ab}/C_{x+c} were measured are presented in this section. Results for the regression analysis between leaf reflectance indices and biochemical constituents, leaf model inversion with PROSPECT on vine leaves, and C_{ab} estimation at canopy level with PROSPECT–rowMCRM models through *scaling-up* methods are described.

5.1. Relationships between optical indices and C_{ab} for V. vinifera L. leaves

Results of the relationships found between 45 narrow-band optical indices calculated from leaf reflectance spectra (Table 4), and biochemical constituents C_a, C_b, C_{ab}, C_{x+c} and ratios

Table 6
Determination coefficients (r^2) found for linear relationships (left on each cell), exponential (center) and 3rd order polynomial (right) between leaf optical indices and biochemical constituents ($n=605$)

	C_a	C_b	C_{ab}	C_{x+c}	C_a/C_b	C_a/C_{x+c}	C_b/C_{x+c}	C_{ab}/C_{x+c}
NDVI	0.26 0.52 0.37	0.23 0.43 0.35	0.26 0.50 0.37	0.25 0.41 0.31	0.05 0.09 0.08	0.37 0.48 0.48	0.18 0.22 0.31	0.33 0.41 0.45
RDVI	0.34 0.60 0.56	0.31 0.50 0.54	0.33 0.58 0.57	0.33 0.50 0.51	0.05 0.09 0.08	0.40 0.50 0.53	0.20 0.24 0.35	0.36 0.44 0.50
SR	0.36 0.56 0.37	0.34 0.52 0.35	0.36 0.56 0.37	0.31 0.42 0.31	0.01 0.02 0.07	0.46 0.53 0.49	0.29 0.33 0.31	0.44 0.50 0.46
MSR	0.34 0.58 0.36	0.32 0.52 0.35	0.34 0.57 0.36	0.30 0.44 0.31	0.02 0.04 0.08	0.46 0.54 0.48	0.26 0.31 0.31	0.42 0.50 0.45
G	0.53 0.32 0.60	0.50 0.36 0.57	0.53 0.34 0.60	0.44 0.32 0.51	0.00 0.00 0.04	0.27 0.20 0.39	0.23 0.20 0.26	0.28 0.21 0.37
ZM	**0.89 0.83 0.89**	**0.84 0.82 0.84**	**0.89 0.84 0.89**	**0.76 0.74 0.76**	0.00 0.00 0.04	0.68 0.64 **0.75**	0.45 0.46 0.47	0.65 0.62 **0.71**
VOG_1	**0.89 0.84 0.89**	**0.84 0.82 0.84**	**0.89 0.85 0.89**	**0.76 0.74 0.76**	0.00 0.01 0.05	0.69 0.65 **0.75**	0.46 0.46 0.47	0.66 0.63 **0.71**
VOG_2	**0.87 0.76 0.87**	**0.82 0.76 0.82**	**0.87 0.78 0.87**	**0.73** 0.69 **0.73**	0.00 0.00 0.03	0.63 0.57 **0.74**	0.43 0.43 0.46	0.60 0.56 0.69
VOG_3	**0.86 0.75 0.87**	**0.82 0.75 0.83**	**0.87 0.76 0.87**	**0.73** 0.68 **0.74**	0.00 0.00 0.03	0.62 0.56 **0.74**	0.42 0.42 0.47	0.59 0.55 0.69
GM_1	**0.87 0.82 0.88**	**0.84 0.82 0.84**	**0.88 0.84 0.88**	**0.76 0.74 0.76**	0.00 0.00 0.05	0.66 0.62 **0.73**	0.45 0.45 0.47	0.63 0.61 0.69
GM_2	**0.81 0.85 0.82**	**0.77 0.82 0.78**	**0.81 0.85 0.82**	0.69 **0.73 0.70**	0.00 0.01 0.05	**0.70** 0.68 **0.73**	0.46 0.48 0.46	0.66 0.66 0.69
CTR_1	0.16 0.25 0.22	0.14 0.22 0.20	0.16 0.25 0.22	0.15 0.20 0.20	0.01 0.02 0.02	0.19 0.22 0.25	0.09 0.12 0.14	0.17 0.20 0.23
CTR_2	0.41 **0.71** 0.65	0.37 0.61 0.61	0.41 0.69 0.65	0.38 0.56 0.55	0.05 0.09 0.09	0.52 0.64 0.66	0.27 0.33 0.42	0.47 0.57 0.62
RGI	0.35 0.12 0.54	0.35 0.17 0.53	0.35 0.14 0.55	0.27 0.14 0.48	0.02 0.03 0.06	0.12 0.06 0.29	0.14 0.11 0.20	0.14 0.08 0.28
BGI_1	0.10 0.10 0.14	0.09 0.09 0.13	0.09 0.10 0.14	0.08 0.08 0.13	0.00 0.000 0.00	0.08 0.08 0.10	0.05 0.05 0.06	0.07 0.07 0.10
BGI_2	**0.77** 0.64 **0.77**	**0.72** 0.64 **0.72**	**0.77** 0.65 **0.77**	0.66 0.59 0.66	0.00 0.00 0.00	0.51 0.46 0.58	0.35 0.35 0.39	0.49 0.45 0.56
BRI_1	0.01 0.02 0.02	0.00 0.02 0.01	0.01 0.02 0.02	0.00 0.01 0.01	0.00 0.00 0.00	0.02 0.03 0.03	0.01 0.01 0.01	0.02 0.02 0.02
BRI_2	0.35 0.53 0.36	0.31 0.46 0.31	0.35 0.52 0.35	0.33 0.42 0.33	0.03 0.05 0.05	0.40 0.46 0.44	0.21 0.25 0.23	0.36 0.42 0.39
CUR	0.33 0.41 0.33	0.30 0.40 0.30	0.33 0.41 0.33	0.27 0.31 0.28	0.00 0.00 0.01	0.36 0.39 0.38	0.24 0.28 0.24	0.35 0.38 0.36
LIC_1	0.23 0.48 0.33	0.21 0.38 0.31	0.23 0.46 0.33	0.23 0.38 0.29	0.05 0.10 0.08	0.32 0.42 0.43	0.15 0.18 0.27	0.28 0.36 0.41
LIC_2	0.25 0.39 0.28	0.22 0.34 0.24	0.25 0.38 0.27	0.23 0.31 0.26	0.02 0.04 0.06	0.30 0.35 0.37	0.15 0.19 0.19	0.27 0.32 0.33
LIC_3	0.08 0.21 0.10	0.08 0.17 0.09	0.08 0.20 0.10	0.08 0.17 0.10	0.02 0.04 0.08	0.14 0.19 0.17	0.06 0.08 0.08	0.12 0.16 0.15
SIPI	0.36 0.62 0.43	0.34 0.54 0.42	0.36 0.61 0.44	0.33 0.48 0.37	0.03 0.06 0.08	0.47 0.56 0.51	0.26 0.31 0.34	0.43 0.51 0.49
PRI_1	0.41 0.34 0.44	0.40 0.37 0.42	0.41 0.36 0.44	0.25 0.22 0.29	0.01 0.01 0.00	0.43 0.39 0.43	0.32 0.34 0.32	0.43 0.40 0.43
PRI_2	0.13 0.02 0.17	0.13 0.04 0.16	0.13 0.03 0.17	0.06 0.01 0.11	0.01 0.01 0.05	0.07 0.03 0.13	0.07 0.06 0.09	0.07 0.04 0.12
PRI_3	0.35 0.44 0.36	0.34 0.44 0.34	0.36 0.45 0.36	0.23 0.27 0.23	0.01 0.00 0.01	0.49 0.51 0.50	0.34 0.38 0.34	0.48 0.50 0.48
NPCI	0.04 0.11 0.05	0.03 0.08 0.04	0.03 0.11 0.05	0.03 0.08 0.06	0.03 0.04 0.05	0.09 0.12 0.11	0.02 0.04 0.03	0.07 0.09 0.08
SRPI	0.03 0.09 0.05	0.02 0.06 0.04	0.03 0.08 0.05	0.02 0.06 0.06	0.02 0.03 0.05	0.07 0.10 0.11	0.02 0.03 0.03	0.06 0.08 0.08
NPQI	0.01 0.01 0.01	0.00 0.01 0.01	0.01 0.01 0.00	0.01 0.01 0.00	0.01 0.00 0.01	0.01 0.01 0.01	0.01 0.01 0.01	0.01 0.01 0.01
MCARI	0.66 0.66 **0.79**	0.61 0.67 **0.74**	0.65 0.68 **0.79**	0.54 0.54 0.66	0.00 0.00 0.02	0.60 0.57 0.61	0.40 0.43 0.43	0.57 0.57 0.59
TCARI	**0.74 0.73 0.83**	0.69 **0.74 0.78**	**0.74 0.75 0.83**	0.61 0.60 **0.70**	0.01 0.00 0.01	0.65 0.61 0.65	0.45 0.48 0.45	0.62 0.62 0.62
OSAVI	0.29 0.56 0.47	0.27 0.46 0.45	0.29 0.54 0.47	0.29 0.45 0.41	0.05 0.09 0.08	0.38 0.49 0.52	0.19 0.23 0.34	0.34 0.43 0.49
$MCARI_1$	0.23 0.44 0.31	0.20 0.35 0.29	0.22 0.41 0.31	0.25 0.39 0.32	0.05 0.09 0.08	0.25 0.33 0.28	0.10 0.13 0.16	0.21 0.28 0.25
$MCARI_2$	0.23 0.46 0.34	0.20 0.37 0.31	0.22 0.44 0.34	0.25 0.39 0.34	0.05 0.09 0.08	0.27 0.37 0.32	0.12 0.15 0.19	0.24 0.31 0.30
$MTVI_1$	0.02 0.12 0.09	0.01 0.07 0.07	0.02 0.11 0.08	0.04 0.11 0.10	0.05 0.09 0.08	0.04 0.09 0.11	0.00 0.01 0.03	0.03 0.06 0.09
$MTVI_2$	0.00 0.02 0.01	0.00 0.00 0.08	0.00 0.01 0.02	0.01 0.02 0.07	0.05 0.08 0.08	0.00 0.02 0.06	0.00 0.01 0.04	0.01 0.001 0.03
TVI	0.01 0.04 0.21	0.01 0.01 0.19	0.01 0.03 0.20	0.00 0.03 0.19	0.05 0.09 0.08	0.00 0.03 0.18	0.01 0.01 0.09	0.00 0.01 0.16
MSAVI	0.36 0.62 0.54	0.33 0.53 0.52	0.36 0.61 0.54	0.35 0.51 0.48	0.04 0.08 0.08	0.43 0.53 0.53	0.22 0.27 0.35	0.39 0.47 0.50
MCARI/OSAVI	0.68 **0.82 0.87**	0.62 **0.78 0.81**	0.68 **0.82 0.86**	0.58 0.65 **0.74**	0.01 0.02 0.02	**0.70 0.73 0.72**	0.44 0.49 0.46	0.66 **0.70** 0.68
TCARI/OSAVI	**0.70 0.90 0.89**	0.64 **0.83 0.83**	0.69 **0.90 0.89**	0.62 **0.73 0.77**	0.02 0.04 0.06	**0.72 0.78 0.74**	0.43 0.49 0.47	0.67 **0.74 0.70**
$MCARI_1$/OSAVI	0.16 0.36 0.18	0.14 0.29 0.16	0.15 0.34 0.18	0.13 0.24 0.17	0.03 0.06 0.07	0.30 0.38 0.31	0.15 0.18 0.17	0.27 0.33 0.28
$MCARI_2$/OSAVI	0.09 0.15 0.12	0.09 0.14 0.11	0.10 0.15 0.12	0.06 0.08 0.09	0.00 0.00 0.01	0.18 0.18 0.19	0.12 0.12 0.12	0.17 0.18 0.18
$MTVI_1$/OSAVI	0.44 0.66 0.50	0.41 0.60 0.48	0.44 0.65 0.50	0.37 0.50 0.40	0.02 0.04 0.05	0.56 0.63 0.59	0.33 0.38 0.38	0.52 0.58 0.56
$MTVI_2$/OSAVI	0.60 **0.70** 0.67	0.56 0.69 0.64	0.60 **0.71** 0.67	0.49 0.55 0.53	0.00 0.01 0.03	0.62 0.64 0.64	0.42 0.46 0.44	0.60 0.63 0.62
TVI/OSAVI	0.53 **0.70** 0.62	0.49 0.66 0.60	0.53 **0.70** 0.62	0.45 0.54 0.50	0.01 0.02 0.04	0.59 0.64 0.63	0.37 0.42 0.42	0.56 0.61 0.60

Highlighted are results for $r^2>0.7$.

are shown in Table 6. The determination coefficients obtained for regression analysis using linear, exponential and 3rd order polynomials demonstrate the non-linearity between specific indices and the biochemical constituents. Red edge ratio indices are generally linear, such as the Vogelmann (VOG_2) or ZM index, yielding $r^2=0.87$ and $r^2=0.89$, respectively for C_{ab} (Fig. 9, top). Other indices showed a clear non-linear relationship with C_{ab}, such as those calculated from visible bands only or in addition to red edge wavelengths (OSAVI, $MCARI_1$, $MCARI_2$, MSAVI, PRI_3), and those indices calculated as combined with OSAVI (MCARI/OSAVI, TCARI/OSAVI, etc) (Fig. 9, center for PRI3 and TCARI/OSAVI). The best optical indices for correlation with C_{ab} in *V. vinifera* L. leaves were ZM ($r^2=0.89$, linear), VOG_1 ($r^2=0.89$, linear), VOG_2 ($r^2=0.87$, linear), VOG_3 ($r^2=0.87$, linear), GM_1 ($r^2=0.88$, linear), GM_2 ($r^2=0.85$, exponential), BGI_2 ($r^2=0.77$, linear), MCARI ($r^2=0.79$, 3rd order polynomial), TCARI ($r^2=0.83$, 3rd order polynomial), MCARI/OSAVI ($r^2=0.86$, 3rd order polynomial), and TCARI/OSAVI ($r^2=0.9$, exponential). As expected, indices traditionally used for vegetation monitoring, such as NDVI, SR or MSR did not obtain as good results as red edge and combined indices,

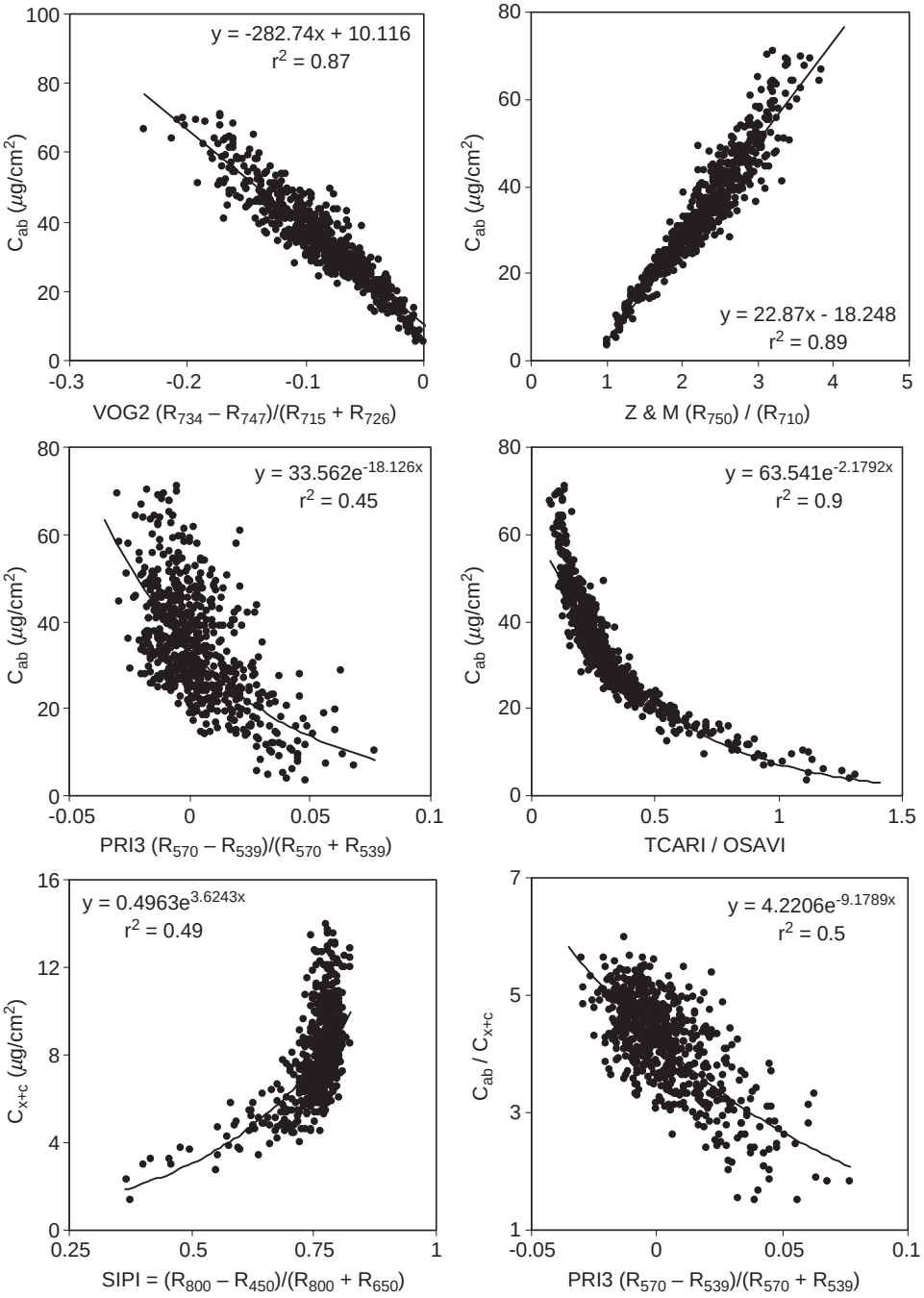

Fig. 9. Relationships obtained between C_{ab} and optical indices calculated from leaf reflectance spectra VOG_2 (upper left) and ZM (upper right), showing a non-linear behavior with PRI_3 (center left) and TCARI/OSAVI (center right), SIPI with C_{x+c} (bottom left) and PRI_3 with C_{ab}/C_{x+c} (bottom right).

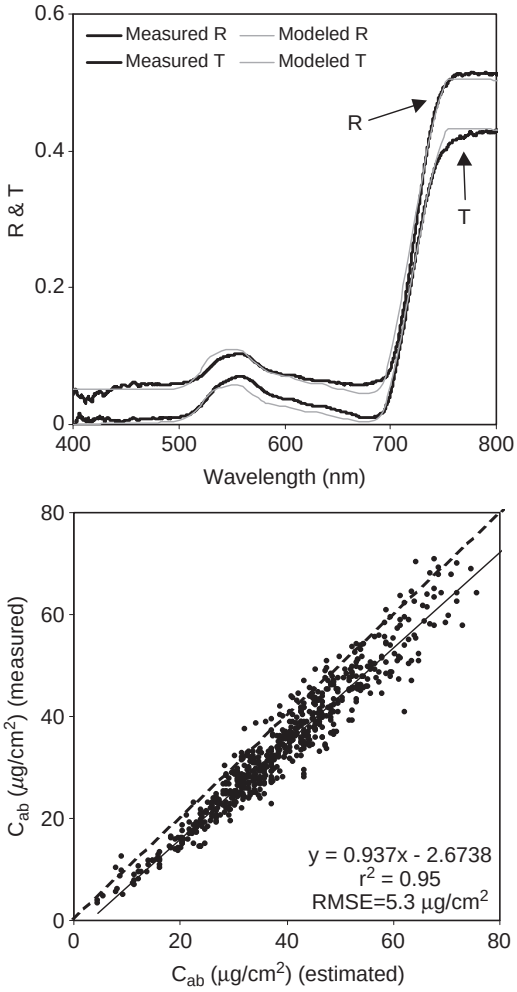

Fig. 10. Leaf reflectance and transmittance spectra measured with the Li-Cor 1800-12 integrating sphere and simulated with PROSPECT (top). Relationship obtained between the C_{ab} measured by destructive sampling and estimated by PROSPECT inversion using the leaf optical properties (bottom).

yielding $r^2=0.5$ (NDVI, exponential), $r^2=0.56$ (SR, exponential), and $r^2=0.57$ (MSR, exponential). Indices developed for maximizing its sensitivity to LAI while decreasing C_{ab} effects, such as $MCARI_2$ and $MTVI_2$ (Haboudane et al., 2004), demonstrated a low relationship with C_{ab}, as expected. Among these structural indices that are demonstrated to be highly related to LAI, $MTVI_2$ was shown in this study to be less affected by C_{ab} variations ($r^2=0.02$) than the $MCARI_2$ index ($r^2=0.44$, exponential).

Regression results for indices and C_{x+c} and ratios C_{ab}/C_{x+c} generally showed poorer relationships, obtaining $r^2=0.49$ for C_{x+c} with SIPI, and $r^2=0.5$ for C_{ab}/C_{x+c} with PRI_3 (Fig. 9, bottom). The PRI index developed for xanthophyll cycle pigment change detection (Gamon et al., 1992) was shown to be more related to the C_{ab}/C_{x+c} ratio ($r^2=0.5$, exponential) than to C_{ab} alone ($r^2=0.45$) and C_{x+c} ($r^2=0.27$). This result agrees with Sims and Gamon (2002) who suggested PRI as a potential indicator for carotenoid/chlorophyll ratio monitoring. With respect to chlorophyll a and b ratios, none of the indices proposed were related to the chlorophyll ratio C_a/C_b, all yielding poor results.

5.2. Estimation of C_{ab} by PROSPECT inversion in *V. vinifera* L. leaves

The *V. vinifera* L. leaf reflectance and transmittance database used for inversion with PROSPECT yielded a good agreement with the modeled spectra, obtaining an average RMSE=0.025 for the 605 leaves (Fig. 10, top). The input variables N, C_{ab} and C_m for PROSPECT, estimated for each leaf spectra by inversion using the iterative optimization method between 400 and 800 nm, yielded average values for the 605 leaves for N ($\mu=1.62$, $\sigma=0.14$), C_{ab} ($\mu=39.4$, $\sigma=13.4$), and C_m ($\mu=0.0035$, $\sigma=0.0012$). The relationship between the measured C_{ab} for each vine leaf, and the PROSPECT-inverted C_{ab} from the optical measurements on the same leaves yielded a determination coefficient of $r^2=0.95$ and RMSE=5.3 µg/cm^2 (Fig. 10, bottom). The PROSPECT model was shown to be valid for simulating the leaf optical properties of *V. vinifera* L. leaves, although a slight overestimation of C_{ab} was found when compared to the 1:1 relationship (yielding the RMSE=5.3 µg/cm^2 mentioned). The RMSE obtained is within the normal range of variation found in similar studies with other species that, in conjunction with the high determination coefficient obtained for this large database, demonstrates the applicability of PROSPECT to simulate the optical properties of *V. vinifera* L. leaves.

5.3. Estimation of C_{ab} by PROSPECT–rowMCRM in *V. vinifera* L. fields

The narrow-band indices that obtained the best relationships in the leaf-level study for C_{ab} estimation, plus the traditional index NDVI (Table 6), were calculated from the 103 sites of 10×10 m imaged by ROSIS and CASI sensors. Relationships were obtained between field-measured C_{ab} and the indices calculated from the airborne reflectance for all pixels falling within the 10×10 m site (pure vine+soil+shadows) and for

Table 7
Determination coefficients (r^2) obtained between ROSIS and CASI airborne optical indices and C_{ab} for the 103 study sites imaged

Indices calculated from ROSIS and CASI images	Chlorophyll content (C_{ab})	
	All pixels (soil+vegetation)	Pure vegetation pixels
NDVI	0.00	0.36
ZM	0.00	0.24
VOG_1	0.00	0.25
VOG_2	0.03	0.31
VOG_3	0.03	0.30
GM_1	0.11	0.07
GM_2	0.00	0.21
CTR_2	0.21	0.14
MCARI	0.40	**0.54**
TCARI	0.43	**0.58**
MCARI/OSAVI	**0.61**	**0.53**
TCARI/OSAVI	**0.59**	**0.55**
$MTVI_2$/OSAVI	0.25	**0.51**
TVI/OSAVI	0.23	0.49

Highlighted are results for $r^2>0.5$.

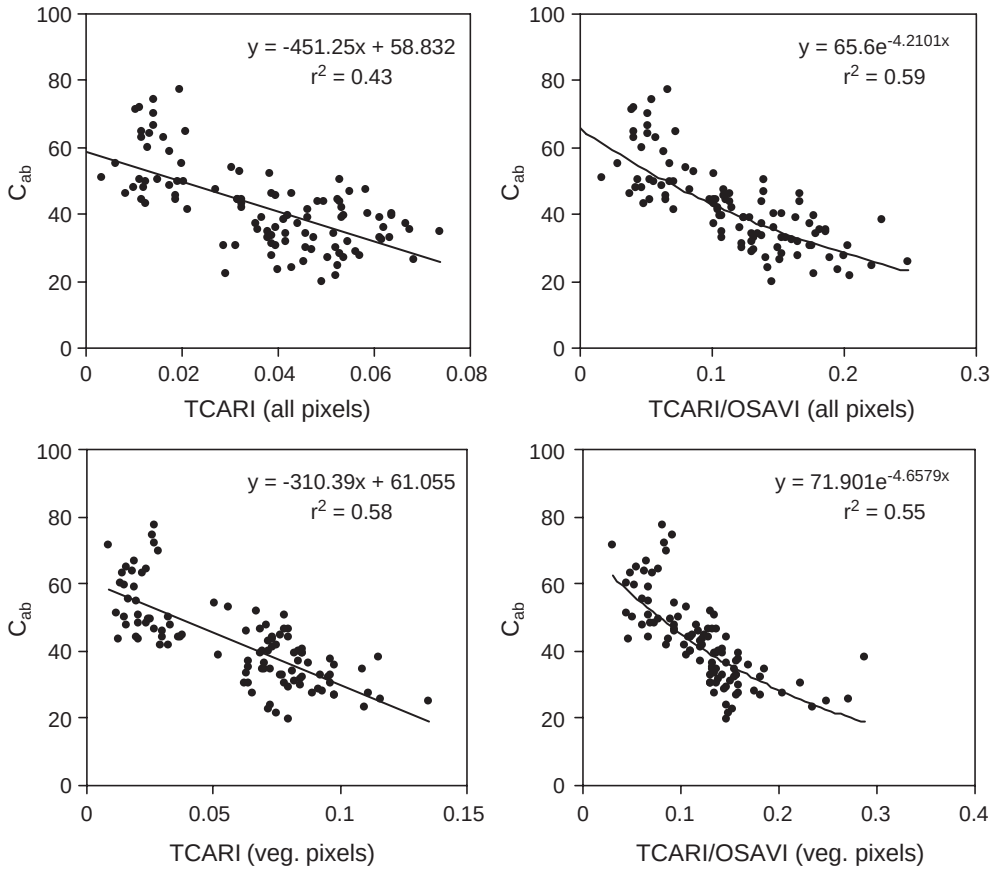

Fig. 11. Relationships obtained between C_{ab} and ROSIS and CASI indices TCARI (top and bottom left), and TCARI/OSAVI (top and bottom right) for aggregated pixels (top left and right) and pure vine pixels (bottom left and right).

the pure vine reflectance only at each study site as extracted with the high-resolution imagery (Table 7). Consistent with previous studies in non-homogeneous crop canopies (Zarco-Tejada et al., 2004), MCARI, TCARI, and combined indices MCARI/OSAVI and TCARI/OSAVI indices yielded the best relationships for both aggregated and pure vegetation pixels. MCARI (TCARI) yielded $r^2=0.40$ ($r^2=0.43$) for aggregated pixels, and $r^2=0.54$ ($r^2=0.58$) for pure vine pixels, showing the effects of soil and shadows on both indices (Fig. 11, top and bottom left for TCARI). Combined indices MCARI/OSAVI and TCARI/OSAVI showed less sensitivity to background effects, as expected, yielding $r^2=0.61$ and $r^2=0.59$ for aggregated pixels, respectively (Fig. 11 top and bottom right for TCARI/OSAVI). The TCARI/OSAVI index showed the greatest consistency when calculated for aggregated and pure vine pixels ($r^2=0.59$ for aggregated pixels; $r^2=0.55$ for pure vine pixels), suggesting this as the most robust narrow-band index for vineyard pigment content monitoring. Other vegetation indices that show significant results at the leaf-level, such as ZM ($r^2=0.89$ at leaf-level), $VOG_{1,\ 2,\ 3}$ ($r^2=0.8$), $GM_{1,\ 2}$ ($r^2=0.8$), and CTR_2 ($r^2=0.69$), were shown to be totally unsuccessful when applied to image-level aggregated pixels due to their high sensitivity to soil background ($r^2\sim0.1$), generating a maximum of $r^2\sim0.3$ when applied to pure vine pixels. The traditional NDVI index, generally used for vegetation biomass and vigor monitoring, yielded $r^2\sim0$ on aggregated pixels and $r^2=0.36$ on pure vine pixels, demonstrating that it is not appropriate for vineyard condition monitoring on non-homogeneous canopies imaged with spatial resolutions lower than 1 m pixel size due to the large background effects and low sensitivity to pigment concentration as indicator of physiological status.

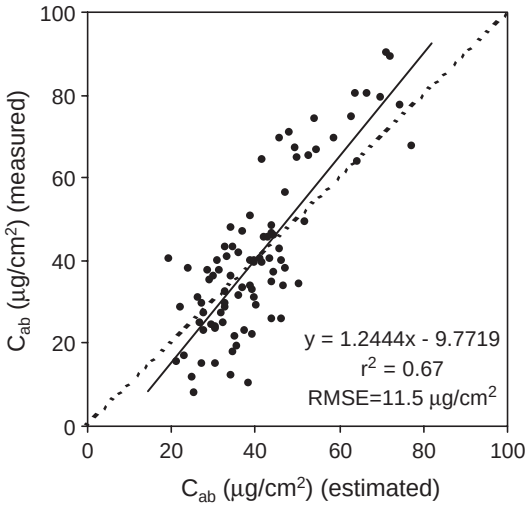

Fig. 12. Estimation of vine C_{ab} at the canopy level by scaling-up TCARI/OSAVI through PROSPECT linked to rowMCRM model.

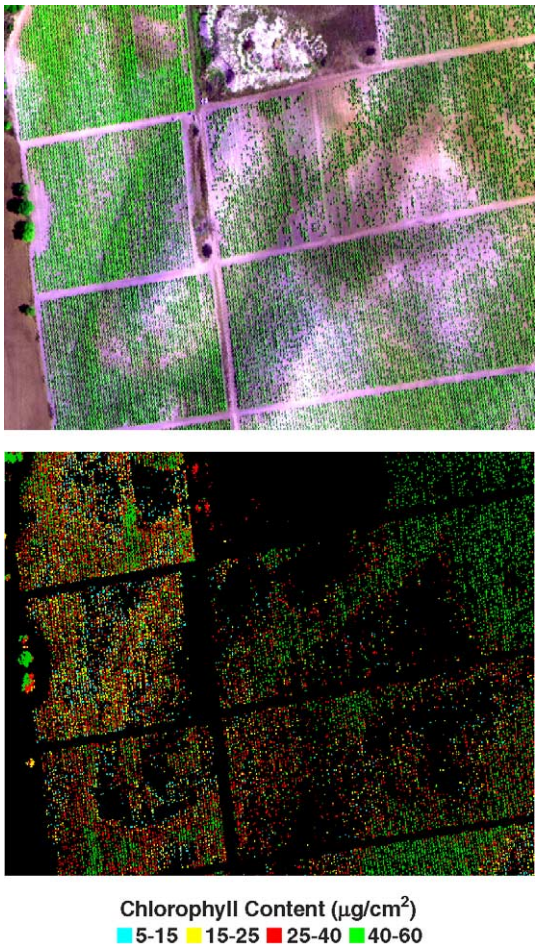

Fig. 13. Airborne CASI image of 1 m spatial resolution and 8 spectral bands (top) showing C_{ab} estimated with TCARI/OSAVI index through PROSPECT–rowMCRM linked models (bottom).

Prediction relationships obtained with PROSPECT–rowMCRM models as explained in the Methods section (Table 5; Fig. 8) when applied to the 103 study sites imaged by ROSIS and CASI airborne sensors yielded $r^2=0.67$ (RMSE=11.5 µg/cm^2) for C_{ab} estimation (Fig. 12). These results at leaf, canopy level for specific indices, and through *scaling-up* methods, suggest the successful retrieval capability of C_{ab} in row-structured vineyard canopies. An example of the natural variability detected in C_{ab} at the vine level in different fields imaged by the CASI sensor in July 2003 can be seen in Fig. 13, illustrating the C_{ab} product in 5 ranges of chlorophyll concentration. The provision of a C_{ab} product map in 5 steps is considered consistent with the RMSE=11.5 µg/cm^2 retrieval accuracy expected.

6. Conclusions

This study investigated the optical properties of *V. vinifera* L. leaves through reflectance and transmittance measurements, optical index calculation, and destructive determination of pigments using a large database of 1467 leaves collected in summer 2002 and 2003. Airborne campaigns imaged a total of 103 study sites from 24 vineyard fields with the ROSIS and CASI hyperspectral sensors at 1 m spatial resolution, studying the validity of optical indices generally used with success in other species at leaf and canopy levels through *scaling-up* simulation with PROSPECT and rowMCRM row-structured canopy reflectance model.

A measurement protocol using a Li-Cor 1800-12 integrating sphere attached to an Ocean Optics model USB2000 fiber spectrometer for stray-light corrected reflectance and transmittance measurements was presented. The measurement protocol consisted of a total of five measurements modifying the position of the collimated light, dark and white plugs of the integrating sphere to measure the reflectance and transmittance signals, reflectance internal standard, reflectance ambient, and dark measurement. The best optical indices for correlation with C_{ab} in *V. vinifera* L. leaves were ZM, VOG_1, VOG_2, VOG_3, GM_1, GM_2, BGI_2, MCARI, TCARI, MCARI/OSAVI, and TCARI/OSAVI (r^2 ranging between 0.8 and 0.9), with poor performance of traditional indices NDVI, SR or MSR. Linear relationships were found between red edge ratio indices such as ZM and VOG indices, whereas generally non-linear relationships were derived with combined indices and ratio indices with visible bands. Results for C_{x+c} and C_{ab}/C_{x+c} ratios yielded $r^2=0.49$ for C_{x+c} with SIPI, and $r^2=0.5$ for C_{ab}/C_{x+c} with PRI_3. The PRI index was shown as a potential indicator for carotenoid/chlorophyll ratio monitoring.

The inversion of PROSPECT model for N, C_{ab}, C_m and C_w estimation, using the large subset database of 605 vine leaf spectra, obtained an averaged RMSE of 0.025, yielding mean values of $N=1.62$, $C_{ab}=39.4$, $C_w=0.02$, and $C_m=0.0035$ ($r^2=0.95$ and RMSE=5.3 µg/cm^2 for C_{ab} estimation by inversion). Therefore these results demonstrate that the PROSPECT leaf model is valid for simulation of the optical properties of vine leaves as function of different pigment levels.

The leaf-level indices that produced the best correlations with C_{ab} were tested at the canopy level on vineyard reflectance spectra extracted from CASI and ROSIS hyperspectral images collected from 103 sites in 24 fields over 2 years. Results at the canopy level demonstrated that MCARI, TCARI, and combined indices MCARI/OSAVI and TCARI/OSAVI indices generated the best relationships for both aggregated and pure vegetation pixels. Combined indices MCARI/OSAVI and TCARI/OSAVI showed less sensitivity to background effects, yielding $r^2=0.61$ and $r^2=0.59$ for aggregated pixels containing pure vine, soil and shadow components. TCARI/OSAVI was the most consistent index for estimating C_{ab} on aggregated and pure vine pixels, yielding $r^2=0.59$ for aggregated pixels and $r^2=0.55$ for pure vine pixels. Physical methods based on PROSPECT linked to rowMCRM model enabled accounting for vineyard structure, row orientation, viewing geometry and background effects, indicating the large effects of the background and vine dimensions on the canopy reflectance. Predictive relationships were developed using PROSPECT–rowMCRM model between C_{ab} and TCARI/OSAVI as function of LAI, using field-measured vine dimensions and image-extracted soil background, row-orientation and viewing geometry. Model-based prediction relationships for C_{ab} content were successfully

applied to the 103 study sites imaged by ROSIS and CASI airborne sensors, yielding $r^2=0.67$ (RMSE=11.5 μg/cm^2).

Results presented in this manuscript indicate the validity of narrow-band indices for C_{ab} estimation and chlorosis detection at the leaf and canopy levels in *V. vinifera* L., demonstrating the validity of PROSPECT and rowMCRM models for leaf and canopy level estimations. This methodology for *scaling-up* leaf-level sensitive indices enabled conclusions to be reached on the effectiveness of biochemical constituent retrievals in canopies where model inversions are complex due to the large number of input parameters required to feed the linked leaf-canopy model.

Acknowledgments

The authors gratefully acknowledge the HySens HS2002-E1 project support provided through the *Access to Research Infrastructures* EU Program. Financial support from the Spanish Ministry of Science and Technology (MCyT) for the project AGL2002-04407-C03, and financial support to P.J. Zarco-Tejada under the *Ramón y Cajal* and *Averroes* Programs are also acknowledged. Financial support from the Natural Sciences and Engineering Research Council (NSERC) of Canada to permit contributions by J.R. Miller is gratefully acknowledged. We thank S. Holzwarth, A. Müeller and the rest of the DLR group, L. Gray and J. Freemantle from York University, and the INTA group for efficient airborne field campaigns with CASI, ROSIS, and DAIS sensors, providing coordination with field data collection. Fertiberia S.A. is acknowledged for providing determinations of foliar nutrients. A. Kuusk and J. Praks are gratefully acknowledged for sharing the rowMCRM code, and E. Vera-Toscano for providing valuable suggestions.

References

Allen, W. A., Gayle, & Richarson, A. J. (1970). Plant canopy irradiance specified by the Duntley equations. *Journal of the Optical Society of America*, *60*(3), 372–376.

Allen, W. A., Gausman, H. W., Richarson, A. J., & Thomas, J. R. (1969). Interaction of isotropic light with compact plan leaf. *Journal of the Optical Society of America*, *59*(10), 1376–1379.

Barnes, J. D. (1992). A reappraisal of the use of DMSO for the extraction and determination of chlorophylls a and b in lichens and higher plants. *Environmental Experimental Botany*, *2*, 85–100.

Ben-Dor, E., & Levin, N. (2000). Determination of surface reflectance from raw hyperspectral data without simultaneous ground data measurements: A case study of the GER 63-channel sensor data acquired over Naan, Israel. *International Journal of Remote Sensing*, *21*, 2053–2074.

Broge, N. H., & Leblanc, E. (2000). Comparing prediction power and stability of broadband and hyperspectral vegetation indices for estimation of green leaf area index and canopy chlorophyll density. *Remote Sensing of Environment*, *76*, 156–172.

Carter, G. A. (1991). Primary and secondary effects of water content of the spectral reflectance of leaves. *American Journal of Botany*, *78*, 916–924.

Carter, G. A. (1994). Ratios of leaf reflectances in narrow wavebands as indicators of plant stress. *International Journal of Remote Sensing*, *15*, 697–704.

Carter, G. A., Dell, T. R., & Cibula, W. G. (1996). Spectral reflectance characteristics and digital imagery of a pine needle blight in the southeastern United States. *Canadian Journal of Forest Research*, *26*, 402–407.

Carter, G. A., & Spiering, B. A. (2002). Optical properties of intact leaves for estimating chlorophyll concentration. *Journal of Environmental Quality*, *31*(5), 1424–1432.

Ceccato, P., Flasse, S., Tarantola, S., Jacquemoud, S., & Gregoire, J. M. (2001). Detecting vegetation leaf water content using reflectance in the optical domain. *Remote Sensing of Environment*, *77*, 22–33.

Chen, J. (1996). Evaluation of vegetation indices and modified simple ratio for boreal applications. *Canadian Journal of Remote Sensing*, *22*, 229–242.

Danson, F. M., Steven, M. D., Malthus, T. J., & Clarck, J. A. (1992). High-spectral resolution data for determining leaf water content. *International Journal of Remote Sensing*, *13*, 461–470.

Daughtry, C. S. T., Walthall, C. L., Kim, M. S., Brown de Colstoun, E., & McMurtrey, J. E. III (2000). Estimating corn leaf chlorophyll concentration from leaf and canopy reflectance. *Remote Sensing of the Environment*, *74*, 229–239.

Dobrowski, S. Z., Ustin, S. L., & Wolpert, J. A. (2002). Remote estimation of vine canopy density in vertically shoot-positioned vineyards: determining optimal vegetation indices. *Australian Journal of Grape and Wine Research*, *8*(2), 117–125.

Dobrowski, S. Z., Ustin, S. L., & Wolpert, J. A. (2003). Grapevine dormant pruning weight prediction using remotely sensed data. *Australian Journal of Grape and Wine Research*, *9*(3), 177–182.

Fernandez-Escobar, R., Moreno, R., & Garcia-Creus, M. (1999). Seasonal changes of mineral nutrients in olive leaves during the alternate-bearing cycle. *Scientia Horticulturae*, *82*, 24–45.

Fourty, T., & Baret, F. (1997). Vegetation water and dry matter contents estimated from top-of-the-atmosphere reflectance data: A simulation study. *Remote Sensing of Environment*, *61*(1), 34–45.

Fuentes, D. A., Gamon, J. A., Qiu, H., Sims, D. A., & Roberts, D. A. (2001). Mapping Canadian boreal forest vegetation using pigment and water absorption features derived from AVIRIS sensor. *Journal of Geophysical Research*, *106*, 33565–33577.

Gamon, J. A., Peñuelas, J., & Field, C. B. (1992). A narrow-waveband spectral index that tracks diurnal changes in photosynthetic efficiency. *Remote Sensing of Environment*, *41*, 35–44.

Gamon, J. A., & Surfus, J. S. (1999). Assessing leaf pigment content and activity with a reflectometer. *New Phytologist*, *143*, 105–117.

Gao, B.-C. (1996). NDWI — a normalized difference water index for remote sensing of vegetation liquid water from space. *Remote Sensing of Environment*, *58*, 257–266.

Gitelson, A. A., Gritz, Y., & Merzlyak, M. N. (2003). Relationships between leaf chlorophyll content and spectral reflectance and algorithms for non-destructive chlorophyll assessment in higher plants. *Journal of Plant Physiology*, *160*(3), 271–282.

Gitelson, A. A., & Merzlyak, M. N. (1996). Signature analysis of leaf reflectance spectra: Algorithm development for remote sensing of chlorophyll. *Journal of Plant Physiology*, *148*, 494–500.

Gitelson, A. A., & Merzlyak, M. N. (1997). Remote estimation of chlorophyll content in higher plant leaves. *International Journal of Remote Sensing*, *18*, 2691–2697.

Haboudane, D., Miller, J. R., Pattey, E., Zarco-Tejada, P. J., & Strachan, I. (2004). Hyperspectral vegetation indices and novel algorithms for predicting green LAI of crop canopies: Modeling and validation in the context of precision agriculture. *Remote Sensing of Environment*, *90*(3), 337–352.

Haboudane, D., Miller, J. R., Tremblay, N., Zarco-Tejada, P. J., & Dextraze, L. (2002). Integration of hyperspectral vegetation indices for prediction of crop chlorophyll content for application to precision agriculture. *Remote Sensing of Environment*, *81*(2–3), 416–426.

Hall, A., Lamb, D. W., Holzapfel, B., & Louis, J. (2002). Optical remote sensing applications in viticulture — A review. *Australian Journal of Grape and Wine Research*, *8*(1), 36–47.

Hall, A., Louis, J., & Lamb, D. (2003). Characterising and mapping vineyard canopy using high-spatial-resolution aerial multispectral images. *Computers and Geosciences*, *29*, 813–822.

Harron, J. (2000). Optical properties of phytoelements in conifers. MSc. Thesis, York University, Toronto, Canada.

Horler, D. N. H., Dockray, M., & Barber, J. (1983). The red edge of plant leaf reflectance. *International Journal of Remote Sensing*, *4*(2), 273–288.

Huete, A. R. (1988). A soil-adjusted vegetation index (SAVI). *Remote Sensing of the Environment*, *25*, 295–309.

Jacquemoud, S., & Baret, F. (1990). Prospect: A model of leaf optical properties spectra. *Remote Sensing of Environment*, *34*, 75–91.

Jacquemoud, S., Ustin, S. L., Verdebout, J., Schmuck, G., Andreoli, G., & Hosgood, B. (1996). Estimating leaf biochemistry using the PROSPECT leaf optical properties model. *Remote Sensing of Environment*, *56*, 194–202.

Johnson, L. F. (2003). Temporal stability of an NDVI–LAI relationship in a Napa Valley vineyard. *Australian Journal of Grape and Wine Research*, *9*(2), 96–101.

Johnson, L. F., Bosch, D. F., Williams, D. C., & Lobitz, B. M. (2001). Remote sensing of vineyard management zones: Implications for wine quality. *Applied Engineering in Agriculture*, *17*(4), 557–560.

Johnson, L. F., Roczen, D. E., Youkhana, S. K., Nemani, R. R., & Bosch, D. F. (2003). Mapping vineyard leaf area with multispectral satellite imagery. *Computers and Electronics in Agriculture*, *38*, 33–44.

Jolley, V. D, & Brown, J. C. (1994). Genetically controlled uptake and use of iron by plants. In J. A. Manthey, D. E. Crowley, & D. G. Luster (Eds.), *Biochemistry of metal micronutrients in the rhizosphere* (pp. 251–266). Boca Raton: Lewis Publishers.

Jordan, C. F. (1969). Derivation of leaf area index from quality of light on the forest floor. *Ecology*, *50*, 663–666.

Kim, M. S., Daughtry, C. S. T., Chappelle, E. W., McMurtrey III, J. E., & Walthall, C. L. (1994). *The use of high spectral resolution bands for estimating absorbed photosynthetically active radiation (Apar)*. 6th symp. on physical measurements and signatures in remote sensing. Jan. 17–21, 1994, Val D'Isere, France.

Kuusk, A. (1995). A Markov chain model of canopy reflectance. *Agricultural and Forest Meteorology*, *76*, 221–236.

Kuusk, A. (1995). A fast, invertible canopy reflectance model. *Remote Sensing of Environment*, *51*, 342–350.

Lagacherie, P., Collin-Bellier, C., & Goma-Fortin, N. (2001). Analysing rate and spatial variability of vinestock mortality in a Languedocian vineyard from high resolution aerial photographs. *Journal International des Sciences de la Vigne et du Vin*, *35*(3), 141–148.

Lamb, D. W., Weedon, M. M., & Bramley, R. G. V. (2004). Using remote sensing to predict grape phenolics and colour at harvest in a Cabernet Sauvignon vineyard: Timing observations against vine phenology and optimising resolution. *Australian Journal of Grape and Wine Research*, *10*(1), 46–54.

Lanjeri, S., Melia, J., & Segarra, D. (2001). A multi-temporal masking classification method for vineyard monitoring in central Spain. *International Journal of Remote Sensing*, *16*, 3167–3186.

le Maire, G., François, C., & Dufrêne, E. (2004). Towards universal broad leaf chlorophyll indices using PROSPECT simulated database and hyperspectral reflectance measurements. *Remote Sensing of Environment*, *89*, 1–28.

Lichtenhaler, H. K., Lang, M., Sowinska, M., Heisel, F., & Mieh, J. A. (1996). Detection of vegetation stress via a new high resolution fluorescence imaging system. *Journal of Plant Physiology*, *148*, 599–612.

Li-Cor Inc. (1984), *Li-Cor model 1800-12 integrating sphere instruction manual* (Revision 1984). Li-Cor Incorporated, 4421 Superior Street, PO Box 4425 Lincoln Nebraska, USA, Publication No. 8305-0034.

Marschner, H., Romheld, V., & Kissel, M. (1986). Different strategies in higher plants in mobilization and uptake of iron. *Journal of Plant Nutrition*, *9*, 695–713.

Montero, F. J., Meliá, J., Brasa, A., Segarra, D., Cuesta, A., & Lanjeri, S. (1999). Assessment of vine development according to available water resources by using remote sensing in La Mancha, Spain. *Agricultural Water Management*, *40*, 363–375.

O'Neill, N. T., Zagolski, F., Bergeron, M., Royer, A., Miller, J. R., & Freemantle, J. (1997). Atmospheric correction validation of CASI images acquired over the BOREAS southern study area. *Canadian Journal of Remote Sensing*, *23*, 143–162.

Peñuelas, J., Filella, I., Lloret, P., Muñoz, F., & Vilajeliu, M. (1995). Reflectance assessment of mite effects on apple trees. *International Journal of Remote Sensing*, *Vol. 16–14*, 2727–2733.

Peñuelas, J., Gamon, J. A., Fredeen, A. L., Merino, J., & Field, C. B. (1994). Reflectance indices associated with physiological changes in nitrogen- and water-limited sunflower leaves. *Remote Sensing of Environment*, *48*, 135–146.

Peñuelas, J., Piñol, J., Ogaya, R., & Filella, I. (1997). Estimation of plant water concentration by the reflectance water index (R900/R970). *International Journal of Remote Sensing*, *18*, 2869–2875.

Qi, J., Chehbouni, A., Huete, A. R., Keer, Y. H., & Sorooshian, S. (1994). A modified soil vegetation adjusted index. *Remote Sensing of Environment*, *48*, 119–126.

Rondeaux, G., Steven, M., & Baret, F. (1996). Optimization of soil-adjusted vegetation indices. *Remote Sensing of Environment*, *55*, 95–107.

Rougean, J. -L., & Breon, F. M. (1995). Estimating PAR absorbed by vegetation from bidirectional reflectance measurements. *Remote Sensing of Environment*, *51*, 375–384.

Rouse, J. W., Haas, R. H., Schell, J. A., Deering, D. W., & Harlan, J. C. (1974). Monitoring the vernal advancements and retrogradation of natural vegetation. *NASA/GSFC final report*. MD, USA: Greenbelt 371 pp.

Schultz, H. R. (1996). Leaf absorptance of visible radiation in *Vitis vinifera* L.: Estimates of age and shade effects with a simple field method. *Scientia Horticulturae*, *66*(1-2), 93–102.

Sims, D. A., & Gamon, J. A. (2002). Relationships between leaf pigment content and spectral reflectance across a wide range of species, leaf structures and developmental stages. *Remote Sensing of Environment*, *81*, 337–354.

Tagliavini, M., & Rombolà, A. D. (2001). Iron deficiency and chlorosis in orchard and vineyard ecosystems. *European Journal of Agronomy*, *15*, 71–92.

Vogelmann, J. E., Rock, B. N., & Moss, D. M. (1993). Red edge spectral measurements from sugar maple leaves. *International Journal of Remote Sensing*, *14*, 1563–1575.

Wallace, A. (1991). Rational approaches to control of iron deficiency other than plant breeding and choice of resistant cultivars. *Plant Soil*, *130*, 281–288.

Wellburn, A. R. (1994). The spectral determination of chlorophylls a and b, as well as total carotenoids using various solvents with spectrophotometers of different resolutions. *Journal of Plant Physiology*, *144*, 307–313.

Zarco-Tejada, P. J., Berjón, A., Morales, A., Miller, J. R., Agüera, J., Cachorro, V., et al. (2003). Leaf biochemistry estimation on EU high-value crops with ROSIS and DAIS hyperspectral data and radiative transfer simulation. *3rd EARSeL workshop on imaging spectroscopy* (pp. 597–602). Germany: Munich.

Zarco-Tejada, P. J., Miller, J. R., Mohammed, G. H., & Noland, T. L. (2000). Chlorophyll fluorescence effects on vegetation apparent reflectance: I. Leaf-level measurements and simulation of reflectance and transmittance spectra. *Remote Sensing of Environment*, *74*(3), 582–595.

Zarco-Tejada, P. J., Miller, J. R., Mohammed, G. H., Noland, T. L., & Sampson, P. H. (2001). Scaling-up and model inversion methods with narrow-band optical indices for chlorophyll content estimation in closed forest canopies with hyperspectral data. *IEEE Transactions on Geoscience and Remote Sensing*, *39*(7), 1491–1507.

Zarco-Tejada, P. J., Miller, J. R., Morales, A., Berjón, A., & Agüera, J. (2004). Hyperspectral indices and model simulation for chlorophyll estimation in open-canopy tree crops. *Remote Sensing of Environment*, *90*(4), 463–476.

Zarco-Tejada, P. J., Whiting, M., & Ustin, S. L. (2005). Temporal and spatial relationships between within-field yield variability in cotton and high-spatial hyperspectral remote sensing imagery. *Agronomy Journal*, *Vol. 97*(No. 3), 641–653.